*Satellite Image Atlas of Glaciers of the World*

*State of the Earth's Cryosphere at the Beginning of the 21st Century*

Sea Ice

*By* Claire L. Parkinson and Donald J. Cavalieri

Cryospheric Sciences Branch, NASA Goddard Space Flight Center

**Abstract**

Sea ice covers vast areas of the polar oceans, with ice extent in the Northern Hemisphere ranging from approximately 7 x $10^6$ $km^2$ in September to approximately 15 x $10^6$ $km^2$ in March and ice extent in the Southern Hemisphere ranging from approximately 3 x $10^6$ $km^2$ in February to approximately 18 x $10^6$ $km^2$ in September. These ice covers have major impacts on the atmosphere, oceans, and ecosystems of the polar regions, and so as changes occur in them there are potential widespread consequences. Satellite data reveal considerable interannual variability in both polar sea ice covers, and many studies suggest possible connections between the ice and various oscillations within the climate system, such as the Arctic Oscillation, North Atlantic Oscillation, and Antarctic Oscillation, or Southern Annular Mode. Nonetheless, statistically significant long-term trends are also apparent, including overall trends of decreased ice coverage in the Arctic and increased ice coverage in the Antarctic from late 1978 through the end of 2003, with the Antarctic ice increases following marked decreases in the Antarctic ice during the 1970s. For a detailed picture of the seasonally varying ice cover at the start of the 21st century, this chapter includes ice concentration maps for each month of 2001 for both the Arctic and the Antarctic, as well as an overview of what the satellite record has revealed about the two polar ice covers from the 1970s through 2003.

## 1. Introduction

### *a. Areal coverage*

Sea ice spreads over vast regions of the Earth's surface at any moment, with major impacts on local climates and ecosystems. Globally, its areal extent ranges from approximately 18 x $10^6$ $km^2$ to approximately 27 x $10^6$ $km^2$, with the distribution of the ice amounts between the Northern and Southern Hemispheres varying systematically with season.

In the Northern Hemisphere, sea ice covers about 15 x $10^6$ $km^2$ at its winter maximum in February and March, spreading throughout the Arctic Ocean, Canadian Archipelago, Hudson Bay, Baffin Bay, and the Kara Sea, and extending also well into the Sea of Okhotsk, the Bering Sea, the Labrador Sea, and the Greenland Sea. This vast ice coverage is reduced in summer by about half, down to approximately 7 x $10^6$ $km^2$ by mid-September, at its summer minimum, when it is confined mostly to the Arctic Ocean itself (Figure 1). The winter maximum sea ice extent is 1.5 times the area of Canada, and even at the summer minimum the ice extent exceeds the combined areas of India, Pakistan, Afghanistan, Iran, and Iraq. Ice thicknesses tend to be under 6 m, with average ice thicknesses in the central Arctic probably in the range of 2-4 m (see Rothrock and others, 1999, and Winsor, 2001, for limited submarine-based ice thickness data) and in the surrounding seas and bays probably under 2 m; ice thicknesses are considerably harder to measure on a hemispheric basis than ice extents and are consequently much less well established.

In the Southern Hemisphere, winter sea ice extent is even greater than in the Northern Hemisphere, peaking at approximately 18 x $10^6$ $km^2$, usually in September, although by the summer minimum, generally in late February, the ice cover decreases to only about 3 x $10^6$ $km^2$ (Figure 2). The much greater annual cycle in the Antarctic than the Arctic results from the different geographical distribution of land/ocean coverage in the two hemispheres. In the Northern Hemisphere the central polar region is occupied by the Arctic Ocean and is largely surrounded by land (Figure 1). The surrounding land areas restrict the expansion of sea ice in winter but also help maintain a large perennial ice cover by restricting the input of warm water in summer. In contrast, in the Southern

Hemisphere the central polar region is occupied by the Antarctic continent, which is surrounded by vast ocean areas largely uninterrupted by land masses (Figure 2). Hence any summer sea ice in the Southern Hemisphere is ice that has survived the summer heating despite being at latitudes south of 78°S, whereas Southern Hemisphere winter ice is unconstrained by land in its northward expansion. Because of the limited amount of ice that survives the summer, sea ice in the Southern Hemisphere tends, overall, to be thinner than the ice in the Northern Hemisphere, with Southern Hemisphere ice thicknesses generally under 1 m (see, e.g., Worby and others, 1996, 1998, and Jeffries and others, 1998).

*b. Climate impacts*

The vast sea ice covers in the two polar regions have many climatological and ecosystem impacts. Climatologically, the ice provides insulation between the ocean and atmosphere, reflects much of the solar radiation incident on it, rejects salt and relatively fresh water to the upper layer of the ocean, and transports cold, relatively fresh water equatorward.

The insulation effect is one of the most important, restricting ocean-atmosphere exchanges of heat, mass, and momentum. The heat insulation is particularly important in winter, when the ice cover greatly restricts loss of heat from the ocean to the very cold polar atmosphere. Maykut (1978) calculated the January sensible heat flux from the ocean to the atmosphere in the central Arctic to be approximately 550 $Wm^{-2}$ in areas where there is direct contact between the ocean and the atmosphere but under 50 $Wm^{-2}$ where the two are separated by an ice layer of 80 cm and down to 0 $Wm^{-2}$ where they are separated by an ice layer as thick as 3 m. His calculations for latent heat flux in January indicate a flux of about 145 $Wm^{-2}$ for an ice-free ocean area, reduced to under 10 $Wm^{-2}$ for an ice cover of 40 cm.

Another important effect of the ice is the reflection of solar radiation. Ice-free ocean tends to have a low albedo, typically somewhere in the range of 3-15%. Ice, on the other hand, tends to have a much higher albedo, especially if covered by a layer of fresh snow, when the albedo can be as high as

98%. More typically, the ice albedo is in the range of 40-80%, but even that is significantly higher than the ocean albedo. The contrast between ice and liquid water albedos leads to an important positive feedback in the climate system: With warming, the sea ice cover is expected to retreat, creating a reduced overall surface albedo and hence an increased absorption of solar radiation and consequently a further warming. Similarly, cooling leads to ice expansion, increased albedo, decreased absorption of solar radiation, and further cooling. A similar positive feedback applies to land ice and snow covers as well, together creating a mechanism that encourages enhanced climate change in the polar regions, where ice and snow covers are widespread.

As ice forms, some of the original water's salt content is rejected to the water below, with some of the rest collecting into salt pockets within the ice. Additional salt drops out of the ice as the ice ages, due either to gravitational downward migration or to a flushing out of the salt by melt water. This rejection of salt to the upper layer of the ocean during ice formation and aging can have important impacts on ocean circulation if the density profile directly under the ice is weak enough that the addition of the rejected salt leads to overturning. Consequences can include mixed-layer deepening, downwelling, and, in some instances, even bottom-water formation, when the surface water downwells to the ocean depths. In contrast, as the ice undergoes surface melting during summer, melt water tends to stabilize the upper ocean layer, generally being relatively fresh and low density.

Another climatological impact of sea ice is the effect of the freeze/melt cycle on seasonal temperature contrasts. Because energy is released during freezing, which occurs predominantly during fall and winter, and is absorbed during melt, which occurs predominantly during spring and summer, the freeze/melt cycle contributes to reducing seasonal temperature extremes.

*c. Ecosystem impacts*

Sea ice affects polar life forms in a wide variety of ways. It provides a habitat for many very small organisms, provides a platform for much larger animals, and restricts light transmissions to life in the ocean underneath the ice, while also insulating such life from the cold polar atmosphere.

Even a small polar ice floe can be the habitat of an abundance of life, including millions of algae, with a biomass sometimes as high as 100 mg of chlorophyll *a* per $m^2$ (Gradinger, 1995). These algae are eaten by protozoans, crustaceans, and nematodes, all also living within the ice, and having densities that can exceed 100,000 creatures per $m^3$ (Melnikov, 1997). Within the Arctic sea ice, rotifers and nematodes are abundant, whereas the dominant metazoan fauna within the Antarctic ice are copepods and acoel turbellarians (Schnack-Schiel, 2003). When sea ice melts in the spring and summer, it releases algae to the surrounding water, at times leading to major algae blooms near the ice edge (e.g., Arrigo and others, 2002).

Sea ice also impacts much larger life forms, many of which take advantage of the platform that the ice provides. In both polar regions, seals give birth and nurse their young on sea ice floes, plus rest and find safely from whales. In the Arctic, polar bears and Arctic foxes wander the ice, with polar bears sometimes staying on the ice for months at a time (Stirling and Derocher, 1993). In the Antarctic, the most noted wanders on the ice are instead penguins, although in both polar regions there are many mammal and bird species frequenting the ice and significantly impacted by it (Ainley and others, 2003). As the ice cover changes, whether due to climate warming or other reasons, the surrounding ecosystems must adjust as well (e.g., Croxall and others, 2002; Derocher and others, 2004).

Sea ice also impacts humans in additional ways, for instance hindering shipping operations, complicating the interpretation of submarine acoustics, and serving as a platform for ice fishing and for scientific measurements.

## 2. Sea Ice Records

Many data products detailing various aspects of the polar sea ice covers are now available; and in this section we discuss some of the more important of these.

### *a. Pre-satellite records*

The very nature of polar seas covered with millions of $km^2$ of uneven, broken, and moving sea ice makes these regions particularly inhospitable and not easily navigable. Prior to 1960, any sea ice observations were generally made by observers from coastlines, from ships, and from aircraft. Many of the earliest sea ice data records were made by explorers and seal and whale hunters, although probably the longest sea ice record is the record of the number of weeks per year of ice along the north coast of Iceland, made by local inhabitants, with some data dating back to about 870 and a more complete record since 1600 (Koch, 1945).

Efforts are underway to piece together many of the early records, which are sparse in both spatial and temporal coverage, for the purpose of creating a longer-term perspective than is possible with the satellite observations alone. Among the key compilations completed so far: Walsh and Johnson (1979) compiled Arctic sea ice data for the period 1953-1977, digitizing the data into monthly grids covering most of the Northern Hemisphere sea ice region; Jevrejeva (2001) compiled a long-term time series of the date of ice breakup in the northern Baltic Sea spanning the period 1529-1990; the Arctic and Antarctic Research Institute (AARI) in St. Petersburg, Russia, compiled historical Russian sea ice extent and thickness observations from the beginning of the 20th century for portions of the Arctic marginal seas (Polyakov and others, 2003); Fetterer and Troisi (1997) further processed digitized 10-day Arctic charts of sea ice concentration (percent areal ice coverage) and ice type for 1953-1990, from the AARI data set, to provide a product on the Equal-Area Scalable Earth (EASE) grid; NSIDC (2004) compiled measurements of 23 central Arctic snow and ice parameters from the former Soviet Union's Sever airborne and North Pole drifting station programs, 1928-1989; and Colony and Thorndike (1984) generated ice-drift velocities for the period 1872-1973, from data from drifting ships, manned research stations on ice floes, and data buoys in the Arctic Ocean. Additionally, a comprehensive Joint U.S.-Russian Arctic Sea Ice Atlas compiled in 1996 provides an historical record of sea ice charts and monthly ice motion fields from both Russian and U.S. sources (including ice station, ice buoy, and ice breaker data) from 1950 to 1994 (Arctic Climatology Project, 2000), and a 200-year record of sea ice extent on the Scotian Shelf in the Gulf of St. Lawrence, Canada, has been

generated from ice patrol and shipping reports, local newspaper stories, and lighthouse records (Hill and others, 2002). In some cases, sea ice records have been generated from proxies instead of direct sea ice observations. For instance, Grumet and others (2001) generated a 1000-year record of spring sea ice conditions in the Arctic region of Baffin Bay using sea salt records from an ice core obtained from the Penny Ice Cap on Baffin Island.

With the advent of satellite observations in 1960, more consistent, if not always more complete, data records became possible, and hybrid sea ice data sets combining both pre-satellite and satellite data have been compiled. In particular, Walsh and Chapman (2001) expanded upon the Walsh and Johnson (1979) 1953-1977 record of the Northern Hemisphere ice by adding satellite data for the post-1972 period and additional pre-satellite data, generating a record for the full twentieth century. Additionally, based on aerial reconnaissance and ship and satellite observations over the period 1953-1986, a collection of about 6000 historical sea ice charts showing sea ice extent and compactness in portions of the Alaskan and western Canadian Arctic and the Bering Sea is archived at the U. S. National Snow and Ice Data Center (NSIDC) in Boulder, Colorado (Dehn, 2002).

*b. Satellite visible and infrared records*

The first U.S. environmental satellite, the Television and Infrared Observation Satellite (TIROS), was launched by NASA on April 1, 1960 and provided the first visible and infrared images of the Earth's surface and its cloud cover. The early TIROS satellites were in orbits of relatively low inclination (angle with the Equator) and hence sea ice observations were limited to latitudes equatorward of about 60°.

In spite of the serious problem of cloud cover, satellite visible and infrared imagery provided the first glimpses of both polar sea ice covers from space. In 1963 photographs of sea ice in the Labrador Sea from TIROS V and VI became the first satellite photographs to be used in an official advisory for ships (Massom, 1991). In 1964 NASA's Nimbus 1 satellite was the first to be placed in a polar orbit (98.6 ° inclination), and this allowed it to provide nearly complete global coverage.

Beginning with TIROS 9 in 1965, many subsequent environmental satellites have been placed in polar orbits.

The TIROS series of satellites was followed by the Environmental Satellite Service Administration (ESSA) series, named for the government agency that operated the satellites, and the Nimbus and National Oceanic and Atmospheric Administration (NOAA) series. The first satellite in the ongoing NOAA series, NOAA 1, was launched in December 1970; and NOAA 17 was launched in June 2002.

A major advance in sea ice remote sensing was made with the launch of the Advanced Very High Resolution Radiometer (AVHRR) on the TIROS-N satellite in 1978. AVHRR provided both improved spectral and improved spatial resolution over previous radiometers. More recent satellites in the NOAA series have also carried AVHRRs, which have provided sea ice imagery at a resolution at nadir of 1.1 km. Under clear sky conditions, this sensor with its wide swath has proved quite useful for creating sea ice charts (e.g., Figure 3). NSIDC archives a variety of gridded sea ice products derived from AVHRR data, including a polar 1 km resolution Level 1b data set useful for monitoring melt ponds on sea ice. Among the gridded data sets are daily sea ice motion vectors for both polar regions spanning the period November 1978 - March 2003 (Fowler, 2003). Sea ice surface temperature is also derived from AVHRR data and is archived as part of NSIDC's Polar Pathfinder EASE-grid composites (NSIDC, 1999; Key and Haefliger, 1992).

The first satellite series designed specifically to monitor the Earth's surface was the Earth Resources Technology Satellite-1 (ERTS-1), launched in July 1972 and later renamed Landsat 1. Since 1972 there have been six more Landsat satellites launched. The most recent, Landsat 7, was launched in 1999 and carries the Enhanced Thematic Mapper Plus (ETM+) sensor, which is an improved version of the Thematic Mapper flown on Landsat 4 and 5 and the Enhanced Thematic Mapper on Landsat 6. ETM+ measures radiances from visible to infrared wavelengths in six spectral bands at a spatial resolution of 30 m. A seventh, panchromatic band provides a resolution of 15 m. The Landsat series of visible and infrared observations has been used widely over the years for studying

the movement and deformation of sea ice, sea ice type, and sea ice concentration (e.g., Figure 4), and for generating regional sea ice atlases (e.g., Ito, 1982).

Later in the series of visible and infrared sensors is the Moderate Resolution Imaging Spectroradiometer (MODIS) designed to measure biological and physical processes on the Earth and in its atmosphere. The first MODIS was launched on NASA's Earth Observing System (EOS) satellite Terra in December 1999, and the second MODIS was launched on the EOS Aqua satellite in May 2002. MODIS provides visible, near-infrared, and infrared imagery in 36 bands within the wavelength range of 0.4 - 14.5 μm. The MODIS sea ice products from both Terra and Aqua are sea ice extent and sea ice surface temperature and are available as Level 2 swath data and as Level 3 gridded data. The MODIS sea ice extent algorithm distinguishes sea ice from open ocean based on reflective characteristics. Thermal data are used to derive ice surface temperature (Hall and others, 2004). Global sea ice extent and ice surface temperature are mapped daily at 1 km and 0.05-degree spatial resolutions, respectively. Eight-day composite data are available at 1-km resolution and are planned for the 0.05-degree resolution product. These products are archived at NSIDC. More detailed information on MODIS sea ice products can be obtained from the MODIS sea ice products user guide (Riggs and others, 2003).

A serious limitation with visible and infrared satellite images is that cloud cover obscures the surface. This problem has been largely overcome through the development of microwave sensors - both active and passive. Furthermore, the microwave sensors have the additional advantage over visible imagery of not needing daylight conditions, as the microwave radiation is emitted either from the satellite instrument (in the case of active-microwave instruments) or from the Earth/atmosphere system (in the case of passive-microwave instruments).

*c. Satellite active-microwave and laser records*

Radar Altimeters and Scatterometers

Active-microwave sensors transmit and receive back a microwave signal and depend on surface backscatter for determining geophysical properties of the surface. These sensors include radar altimeters, scatterometers, side-looking real aperture radars, and synthetic aperture radars. The primary difference between radar altimeters and scatterometers is that the altimeter is a nadir-pointing sensor and collects data along a narrow beam, whereas the scatterometer collects data within a swath centered on the satellite track. The primary applications of these sensors have been in oceanographic studies, providing, for example, information on ocean topography and on wind speed and direction directly above the ocean surface. The first spaceborne radar altimeter and scatterometer flew onboard Skylab in 1973 and 1974, but it was only after the launch of the Geodetic Earth Orbiting Satellite 3 (GEOS-3) in 1975 that sea ice was recorded by an altimeter from space. Launched in 1983, the Russian satellite COSMOS-1500 carried a real-aperture radar that was used for navigation through ice infested waters.

The Seasat-A Satellite Scatterometer (SASS) lasted only four months after its launch in June 1978, but it provided a major impetus for using active sensors to study sea ice. Most existing sea ice scatterometer data records are derived from microwave scatterometers onboard the European Remote Sensing (ERS) satellites ERS-1 and ERS-2, launched in 1991 and 1995, respectively, and the Japanese Advanced Earth Observing Satellite-1 (ADEOS-1) and ADEOS-2 satellites, launched in 1998 and 2002, respectively. NASA's Quick Scatterometer (QuikSCAT) was launched in 1999 to provide scatterometry coverage shortly after ADEOS-1 failed. Sources of scatterometer sea ice data include:

• *Centre ERS d'Archivage et de Traitement* (*CERSAT - French ERS Processing and Archiving Facility*). CERSAT is part of the French Research Institute for Exploitation of the Sea (IFREMER) and is the node of the European Space Agency (ESA) for archiving, processing and validating data from spaceborne sensors. Among the products archived are Level 3 products of backscatter coefficients over sea ice for both north and south polar regions, presented on polar stereographic 25-km resolution grids. From these gridded products it is possible to calculate the sea ice extent and to categorize three ice types: multiyear ice, consolidated first-year ice, and marginal ice. Weekly data

products are available from the Active Microwave Instrument (AMI) in its Wind Scatterometer (AMI-Wind) mode on the ERS-1 (5 August 1991 - 26 May 1996) and ERS-2 (25 March 1996 - 15 January 2001) missions; three-day products are available from the NASA Scatterometer (NSCAT) sensor on the ADEOS-1 (19 September 1996 - 29 June 1997) satellite; and daily products at both 12.5 km and 25 km resolutions are available from the SeaWinds sensor on the QuikSCAT (20 July 1999 - 30 June 2001) platform. In addition, three-day and six-day sea ice drift products are available for the central Arctic at a spatial resolution of 62.5 km for the winter (October - April) periods 1999-2000 through 2002-2003. Further details about these products can be found at http://www.ifremer.fr/cersat/en/data/gridded.htm.

• *Brigham Young University (BYU) Center for Remote Sensing.* This Center archives Arctic and Antarctic sea ice extents derived from QuikSCAT and NSCAT. The QuikSCAT data cover the period 19 July 1999 – 7 June 2004 and are available in two formats: a masked image where ocean areas outside the sea ice limit are set to the no-data value, and an ASCII file containing latitude and longitude pairs corresponding to contour points on the ice edge. The NSCAT data cover the period 14 September 1996 - 28 June 1997 and consist of ice masked Scatterometer Image Reconstruction with Filtering (SIRF) images (Long and others, 1993) along with similar ASCII files to those for the QuikSCAT data. A sea ice motion data set derived from a merged scatterometer (QuikSCAT)/passive-microwave (Special Sensor Microwave Imager [SSMI]) product (Liu and others, 1999) is also available at BYU. The ice motion products are available as postscript images of the ice motion and as ASCII files describing the ice motion vectors. Further details of the BYU scatterometer sea ice data sets can be found at http://www.scp.byu.edu/derived.html.

• *The Physical Oceanography Distributed Active Archive Center (PO.DAAC)* at the Jet Propulsion Laboratory, California Institute of Technology. PO.DAAC is the long-term archive of sigma-0 data from most of the spaceborne scatterometers. It also archives the BYU data sets, including daily browse images of QuikSCAT sigma-0 measurements, daily browse images of SeaWinds sigma-0

measurements, and high resolution images of Seasat sigma-0 measurements. The website for PO.DAAC is http://podaac.jpl.nasa.gov/.

Laser Altimeters

An improvement over radar altimeters for estimating sea ice thickness is the laser altimeter, with its higher spatial resolution and better precision. The first laser altimeter in Earth orbit was launched by NASA, as part of the EOS Program, on the Ice, Cloud, and land Elevation Satellite (ICESat) in January 2003. The Geoscience Laser Altimeter System (GLAS) on ICESat was launched primarily to measure ice sheet elevations, but it also provides the potential for monitoring the third dimension of the polar sea ice cover – ice thickness – derived from the measured surface elevation. The Level 2 sea ice elevation data are archived at NSIDC (Zwally and others, 2003).

A European satellite named CryoSat (Wingham and others, 2004) will complement ICESat's sea ice elevation measurements with its newly designed radar altimeter. This mission is designed to measure the thickness variability of both land and sea ice. While the spatial resolution will not be as good as ICESat's, CryoSat will have the advantage of being able to map ice thicknesses through cloud cover. The launch of CryoSat is currently scheduled for 2005.

Synthetic Aperture Radar

Unlike passive-microwave sensors, synthetic aperture radars (SARs) provide narrow swath, very high spatial resolution imagery. Because of their high spatial resolutions and availability under dark or light, cloudy or clear conditions, SAR data are particularly useful for studies of sea ice processes. Spaceborne SARs were launched by the U.S. on Seasat in June 1978 and by Russia on COSMOS-1870 in July 1987. Subsequently other SAR sensors were launched by the Europeans on ERS-1 and ERS-2, the Japanese on the Japanese Earth Resources Satellite-1 (JERS-1), and the Canadians on RADARSAT. The Alaska SAR Facility (ASF) at the University of Alaska, Fairbanks, is under contract to NASA to acquire, process, archive, and distribute SAR data from the European Space Agency ERS-1 and ERS-2 satellites, the Japan Aerospace Exploration Agency (JAXA) JERS-1

satellite, and the Canadian Space Agency RADARSAT-1 satellite. ASF is the primary repository of spaceborne SAR data, including derived sea ice products.

The Geophysical Processor System at ASF produces two sea ice type classification products from the ERS-1 SAR. The sea ice types are classified as multiyear ice, deformed first-year ice, undeformed first-year ice, and new ice/smooth open water. The two products are: 1) sea ice classification images color-coded according to ice type; and 2) files listing the percentage of each sea ice type found in 5 km x 5 km image blocks.

In addition to ice type classification products, the ASF Geophysical Processor System produced and archives sea ice motion vectors from ERS-1 SAR data. During the "ice phases" of ERS-1 operations, the satellite retraced its ground track about every three days, in part to facilitate the determination of ice motions. Each ice motion product gives the initial latitude and longitude of an ice feature and the final latitude and longitude, as well as its displacement in kilometers and its rotation in degrees. About 60 of these products were generated for each winter week from September 1991 until December 1994. Most of the ice motion vectors are for the Beaufort Sea and the high Arctic region up to 85°N latitude, although some are for the Chukchi and East Siberian seas and a few are for areas south of 65°N.

*d. Satellite passive-microwave records*

The most spatially and temporally complete global sea ice data records are provided by passive-microwave satellite observations dating from 1973 to the present, especially those from November 1978 to the present, and those are the records used in Sections 3-5 to depict the state of the sea ice cover. Satellite passive-microwave records are derived from measurements of radiation emitted from within the Earth/atmosphere system and have the advantages of being equally available under dark and light conditions, being unaffected by most cloud cover, and being obtainable near globally at a frequency of every few days or better.

The first passive-microwave observations of the Earth's surface from space were made from the Russian COSMOS 243 satellite in 1968, with a nadir viewing radiometer operating at frequencies of 3.5, 8.8, 22.2, and 37 GHz (Massom, 1991). However, the first spaceborne radiometer to produce images of the polar sea ice covers was the Electrically Scanning Microwave Radiometer (ESMR) on NASA's Nimbus 5 satellite. The ESMR, a single-channel sensor operating at 19 GHz, was launched in December 1972 and continued to provide useful sea ice data for about 4.5 years. The first sea ice atlases based on satellite microwave imagery were created from the ESMR data, for both the Antarctic (Zwally and others, 1983) and the Arctic (Parkinson and others, 1987).

The next major advance in imaging microwave radiometers was provided by the Scanning Multichannel Microwave Radiometer (SMMR) launched on the Nimbus 7 spacecraft in October 1978 (Gloersen and Barath, 1977). The SMMR overcame several limitations of the single-channel ESMR and provided more accurate retrievals of sea ice concentration by covering a range of frequencies from 6.6 GHz to 37 GHz with dual polarization. With polarization and spectral information available, the SMMR data were used to provide not only maps of Arctic and Antarctic sea ice concentrations, but also the first satellite-derived maps of sea ice type and temperature (Cavalieri and others, 1984). With over eight years of observations, November 1978 – August 1987, a SMMR sea ice atlas was produced documenting changes in Arctic and Antarctic sea ice concentration, shifts of Arctic multiyear ice distribution, and sea ice temperature in both polar regions (Gloersen and others, 1992).

In August 1987 the Nimbus 7 SMMR stopped scanning, concluding the SMMR sea ice record. In July of the same year, a scanning microwave radiometer was launched on the operational Defense Meteorological Satellite Program (DMSP) satellite series. This sensor, the Special Sensor Microwave Imager (SSMI), operates at a range of frequencies from 19 GHz to 85 GHz and has been flown on several DMSP satellites since 1987. As of early 2005, the SSMI continues to provide polar data coverage.

One of the first sea ice applications of the DMSP SSMI data was the compilation by the Canadian Atmospheric Environment Service and the Canadian Space Agency of a Northern

Hemisphere sea ice atlas covering the period July 1987 through June 1990 (LeDrew and others, 1992). The atlas documents seasonal and interannual changes in both the total sea ice cover and first-year and multiyear ice types.

Analyses of the SMMR and SSMI satellite microwave data records have revealed large year-to-year variability in the polar ice covers as well as a long-term secular change (see Sections 4 and 5). For the purpose of determining the trends in the Arctic and Antarctic sea ice extents, the generation of a continuous, seamless sea ice record from the various satellite microwave imagers became a top priority. To this end, a multi-year effort was undertaken at NASA Goddard Space Flight Center to blend the sea ice extent records from the SMMR and three SSMIs from 1978 through 1996 (Cavalieri and others, 1997; 1999). Results from these analyses have been published for both hemispheres (Parkinson and others, 1999; Gloersen and others, 1999; Zwally and others, 2002). The SMMR/SSMI time series was further extended back to 1972/73 through the combined use of the four-year ESMR data set and a data set from the National Ice Center (NIC) based on surface, airborne, and satellite visible, infrared, and microwave observations (Cavalieri and others, 2003). All of these time series, including hemispheric and regional sea ice extents and areas for both the Arctic and Antarctic, are archived at NSIDC. Other groups have also analyzed the SMMR/SSMI record, including Johannessen and others (1995), Bjørgo and others (1997), Stammerjohn and Smith (1997), and Watkins and Simmonds (2000).

In May 1999, India launched the Indian Remote Sensing (IRS) satellite IRS P4 (also called Oceansat 1), carrying a Multi-frequency Scanning Microwave Radiometer (MSMR). MSMR provides dual-polarized images of sea ice at four frequencies: 6, 10, 18, and 21 GHz. A research group at the Indian National Centre for Antarctic and Ocean Research in Goa, India, published an atlas of Antarctic sea ice extents based on the sharp contrast between the observed microwave brightnesses between ice-free ocean and ice-covered ocean for the period June 1999 through September 2001 (Vyas and others, 2004).

The next generation passive-microwave imager, the Advanced Microwave Scanning Radiometer for EOS (AMSR-E) (Kawanishi and others, 2003), was designed and built by the Japanese National Space Development Agency (NASDA, which subsequently was merged into JAXA) and was launched on NASA's Aqua satellite in May 2002. AMSR-E operates at a wider range of frequencies (6-89 GHz) than either SMMR or SSMI and provides a higher spatial resolution, about twice that of the SSMI. These AMSR-E attributes have led to the development of more sophisticated passive-microwave sea ice algorithms (Comiso and others, 2003). AMSR-E data, when combined with data from other sensors, promise to yield new information on how the polar sea ice covers interact with the global climate system and, in particular, to provide a better understanding of the role of sea ice in climate feedback mechanisms. Coincident Arctic sea ice images from the Aqua AMSR-E and Aqua MODIS data are shown in Figure 5.

Two passive-microwave radiometers first launched in 2003 will provide additional observations for developing improved sea ice data records. The first is WindSat, a U. S. Navy instrument launched on the Air Force Coriolis satellite in January 2003. A multi-frequency polarimetric microwave radiometer designed primarily for measuring ocean surface wind vectors from space, WindSat also produces fully polarimetric data for studying other geophysical parameters, including sea ice. The WindSat data are archived at PO.DAAC (https://podaac.custhelp.com). Second, the first Special Sensor Microwave Imager Sounder (SSMIS) was launched in October 2003 on a DMSP platform. The SSMIS replaces, enhances, and extends the imaging and sounding capabilities of the DMSP Special Sensor Microwave Temperature sounder (SSMT), SSMT-2, and SSMI microwave sensors (Poe and others, 2001). SSMIS is expected to provide improved atmospheric corrections to sea ice retrievals making use of its atmospheric sounding channels.

In May 1994, the U.S. Congress developed a convergence plan designed to reduce the overall cost of developing and operating polar-orbiting environmental satellite systems, by merging efforts from within NASA and the Departments of Defense and Commerce. This plan led to the ongoing development of the National Polar-orbiting Operational Environmental Satellite System (NPOESS).

The microwave radiometer scheduled to be flown on NPOESS is the Conical-scanning Microwave Imager & Sounder (CMIS) and is expected to be launched in 2010 and to provide improved retrievals through its higher spatial resolution and increased number of channels.

**3. Annual Cycle of Sea Ice**

To depict the state of the sea ice cover at the start of the twenty-first century, recognizing its dramatic seasonal variations, this section provides images of sea ice concentrations for each month of 2001, for both polar regions. These images for the first year of the twenty-first century are accompanied by corresponding images for the 25-year monthly average data for the period 1979-2003 and by plots of the annual cycles of ice extent, defined as the ocean area having ice concentrations of at least 15% (when gridded to pixels of size approximately 25 x 25 km). All the images are derived from the satellite passive-microwave data of the Nimbus 7 SMMR and the DMSP SSMI, using the NASA Team algorithm detailed in Cavalieri and others (1984) and Gloersen and others (1992) and the SMMR/SSMI data set matching procedures described in Cavalieri and others (1999).

*a. Arctic*

Monthly average Arctic sea ice concentration images for each month of 2001 are presented in Figure 6, and the corresponding monthly average images for the 25-year period 1979-2003 are presented in Figure 7. The black circular region centered at the North Pole indicates missing data; because of the respective satellite orbits, the SMMR data do not extend poleward of 84.6°N and the SSMI data do not extend poleward of 87.6°N.

As shown in Figure 7, the Arctic ice cover is typically close to its maximum extent in January, although expands outward a bit further in February and March. During this January – March period, the ice cover tends to be highly compact (over 92% ice concentration) throughout almost the entirety of the Arctic Ocean, Canadian Archipelago, Hudson Bay, Baffin Bay, and the Kara Sea, with ice of lesser concentrations extending well into the Sea of Okhotsk, Bering Sea, Labrador Sea, Greenland Sea, and Barents Sea. As the ice decays in spring and summer, the decay is apparent both in a

lessening of ice concentrations, starting in the marginal seas and progressing to the central Arctic, and in a marked retreat of the ice edge. By the end of summer, at the ice extent minimum in September, the remaining ice is predominantly in the Arctic Ocean, with some ice also in the Canadian Archipelago and the Greenland Sea. The ice cover then, in autumn and early winter, fairly systematically expands back outward to its wintertime distribution (Figure 7). Monthly ice extents averaged over the 25 years range from a minimum of 6.8 x $10^6$ $km^2$ in September to a maximum of 15.3 x $10^6$ $km^2$ in March (Figure 8).

The year 2001, like each of the individual years, had basically the same annual cycle as the 25-year average, although with some differences apparent in each month. Among the prominent differences visible in Figure 6 versus Figure 7: February and March 2001 had more ice in the Sea of Okhotsk than the 1979-2003 average February and March did; April and May 2001 had a less expansive ice cover in the Bering Sea than the average April and May; June and July 2001 had less ice in Hudson Bay than the average June and July; August and September 2001 had less ice in the Greenland Sea and lower concentration ice in much of the central Arctic than the average August and September; October 2001 had somewhat higher concentration ice just north of Alaska and eastern Siberia than the average October; November 2001 had somewhat more ice in the Bering Sea but less ice in the Barents Sea than the average November; and December 2001 had less ice in Hudson Bay than the average December (Figures 6-7). Overall, monthly average ice extents tended to be slightly less in 2001 than in the 25-year average, although even in the month with the largest difference, July, the 2001 ice extent (9.0 x $10^6$ $km^2$) was 93% of the 25-year average July ice extent (9.7 x $10^6$ $km^2$) (Figure 8). The 2001 July extent is outside the 1-standard deviation bounds of the 25-year average (9.7 x $10^6$ $km^2$ ± 0.5 x $10^6$ $km^2$) but not outside the 2-standard deviation bounds.

*b. Antarctic*

Figure 9 presents monthly average Antarctic sea ice concentration images for each month of 2001, and Figure 10 presents the corresponding monthly images for the average of the years 1979-

2003. On average, the ice cover by January has retreated to the Antarctic coast at a few locations around the continent, most prominently in front of the Ross Ice Shelf; and it has retreated to a greater portion of the coast by the time of its minimum, in February. The sea with the largest amount of ice remaining in February is the western Weddell Sea, with much lesser but still sizeable amounts of ice remaining in the Bellingshausen, Amundsen, and eastern Ross seas (Figure 10).

A few coastal polynyas (sizeable regions of open water in the midst of a sea ice cover) are apparent in the 25-year averages for both January and February, and these have generally closed by March, as the ice cover begins its late-summer/early-autumn advance. By April the ice has spread noticeably equatorward around much of the continent and toward the northeast in the western Weddell Sea, in conjunction with the cyclonic ocean currents. By April, the only portion of the coast still free of ice is along the west coast of the Antarctic Peninsula (Figure 10).

The ice cover typically continues to expand outward from May to August, by which time it has reached 55°S in the far eastern Weddell Sea and 60°S – 65°S in the Ross Sea. The ice coverage increases slightly from August to September, although all three months August, September, and October have comparably large ice extents, preceding the substantial decay that takes place over the following three months (Figure 10). The minimum monthly average ice extent is $3.0 \times 10^6$ km$^2$, in February, and the maximum is $18.2 \times 10^6$ km$^2$, in September (Figure 8). Decay, lasting five months, is clearly more rapid than the seven-month ice advance, in contrast to the situation in the Arctic, where the most rapid rates of change occur during the growth period, particularly September-December (Figure 8). In the Antarctic, the rates of decay are greatest from November to December and December to January, with rates of change noticeably greater than those of any other 25-year-average 30-day period in either hemisphere (Figure 8).

As with the Arctic ice cover (Section 3a), although the basic seasonal contrast in the Antarctic ice cover remains valid for each year, details of the cycle vary, as illustrated by the contrasts between the 2001 monthly images (Figure 9) and the 1979-2003 average images (Figures 10). Among the clearly visible contrasts: January 2001 had a more concentrated but less expansive ice cover in the

western Weddell Sea than the 25-year average January did; February and March 2001 had more ice in the western Ross Sea than the 25-year average February and March; April-June 2001 had less expansive ice in the Bellingshausen and Amundsen seas that the average April-June; July and August 2001 had less expansive ice in the vicinity of the Greenwich meridian but more expansive ice at about 80°E than the average July and August; November and December 2001 had noticeably less expansive ice in the western Weddell Sea but more expansive ice in the vicinity of 45°E and the vicinity of 135°W than the average November and December; and December 2001 also had a noticeably larger polynya off the Ross Ice Shelf than the average December (Figures 9-10).

Integrating over each of the images of Figures 9-10, ice extents in 2001 tended to be somewhat greater than the 25-year average in the summer months, but slightly less than the 25-year average in the winter months, with the greatest differences coming in February and March (Figure 8). The February and March 2001 ice extents are $3.6 \times 10^6$ km$^2$ and $4.7 \times 10^6$ km$^2$, respectively, compared to 25-year average values of $3.0 \times 10^6 \pm 0.3 \times 10^6$ km$^2$ and $3.9 \times 10^6 \pm 0.4 \times 10^6$ km$^2$ (i.e., the 2001 ice extents are greater than the 25-year averages by approximately 20% in each of these two months and are about 2 standard deviations away from the respective averages).

Summing the values in the two hemispheres, the annual cycle of global sea ice extents is roughly in phase with the cycle in the Southern Hemisphere ice, reflecting the much larger annual cycle in the Southern Hemisphere than the Northern Hemisphere, although has lesser amplitude, being modulated by the out-of-phase nature of the two ice covers (Figure 8). Global sea ice extent typically (averaged over 1979-2003) varies from a minimum of about $18.2 \times 10^6$ km$^2$ in February to a maximum of about $26.5 \times 10^6$ km$^2$ in October and November (Figure 8). The year 2001 had slightly above average extents in the months February-May but slightly below average ice extents in June-December (Figure 8).

**4. Trends in the Sea Ice Cover**

The prominent annual cycle of sea ice coverage in both polar regions (Section 3) tends to mask any long-term trends when time series of monthly or daily ice extents are plotted. However, trends do exist and can be made visible through various representations of the data. Here we choose to plot the results as monthly deviations and yearly and seasonal averages, as well as monthly averages. Monthly deviations are calculated for each year by taking the individual month's data and subtracting the average of that month's data for the full 25 or 26 years (e.g., February 1983 minus the February average for 1979-2003). Because the SMMR data start at the end of October 1978, we start our monthly average and monthly deviation plots with November 1978 and go through December 2003, so that November and December have 26 years of data, the other months 25 years of data. Yearly and seasonal averages are all 25-year averages, calculated for each year 1979-2003 by averaging the daily average ice extents.

*a. Arctic*

Time series of Northern Hemisphere monthly sea ice extents for November 1978 – December 2003 and monthly deviations for the same time period are plotted in Figures 11a and 11b, respectively; and yearly and seasonal averages for 1979-2003 are plotted in Figure 11c. The dominance of the annual cycle is apparent in Figure 11a, but the existence of a strong trend toward decreasing sea ice coverage is clear in the plots of both the monthly deviations and the yearly averages (Figures 11b and 11c). The slopes of the trend lines are –36,700 ± 2,200 $km^2$/yr for the monthly deviations and –36,600 ± 4,400 $km^2$/yr (-3.0 ± 0.4 %/decade) for the yearly averages; both are statistically significant at the 99% confidence level. These trends are somewhat greater in magnitude than the trends of –34,300 ± 3,700 $km^2$/yr (for monthly deviations) and –34,000 ± 8,300 $km^2$/yr (-2.8 %/decade, for yearly averages) calculated by Parkinson and others (1999) for the same SMMR/SSMI data but for the period November 1978 – December 1996 and the –32,000 ± 4,000 $km^2$/yr trend calculated by Bjørgo and others (1997) for the period November 1978 – August 1995. The higher values for the record through December 2003 (Figure 11) reflect the acceleration of the downward trend in recent years. A similar acceleration is also apparent from the lower values obtained when extending the SMMR/SSMI data set

backward in time through incorporation of the ESMR and NIC data sets (e.g., Cavalieri and others, 2003).

The downward trend in Arctic sea ice coverage is not limited to individual seasons, instead being apparent in all four seasons (Figure 11c). The largest magnitude seasonal slope is –46,100 ± 9,300 $km^2$/yr (-5.4 ± 1.1 %/decade) for summer, but even the smallest, at –28,300 ± 5,100 $km^2$/yr (-1.8 ± 0.3 %/decade) for winter, is statistically significant at the 99% confidence level, as are all four of the seasonal trend values.

The decreasing Arctic sea ice extents revealed by the satellite data (e.g., Figure 11) seem to have been accompanied by decreasing ice thicknesses (e.g., Rothrock and others, 1999, and Wadhams and Davis, 2000). However, ice thickness information has come largely from in situ and submarine measurements, both of which are spotty in both time and space, and some studies have found the data insufficient to conclude either increasing or decreasing trends (e.g., McLaren and others, 1992, for the North Pole for 1977-1990, and Winsor, 2001, for the Arctic during the 1990s). Analysis of additional submarine data and eventual development of an ice thickness data set from satellite altimetry (Zwally and others, 2003; Wingham and others, 2004) should help establish a more definitive record of ice thickness changes.

*b. Antarctic*

Time series of Southern Hemisphere monthly ice extents and deviations for November 1978 – December 2003 and yearly and seasonal averages for 1979-2003 are plotted in Figure 12. The monthly averages highlight the prominent annual cycle (Figure 12a), while the monthly deviations and yearly averages both show the trend toward increasing ice coverage (Figures 12b and 12c). The positive trends, at 11,200 ± 3,100 $km^2$/yr for the monthly deviations and 11,700 ± 5,400 $km^2$/yr (1.0 ± 0.5 %/decade) for the yearly averages, are less than a third of the magnitude of the corresponding negative trends in the Arctic (Section 4a), although are still statistically significant, the monthly deviations at a 99% confidence level and the yearly averages at a 95% confidence level.

Seasonally, the Southern Hemisphere sea ice exhibits positive ice extent trends for the 1979-2003 period for each of the four seasons, although none at a statistically significant level. The strongest positive trend is for the autumn season, with a trend of 22,600 ± 12,500 $km^2$/yr (2.3 ± 1.3 %/decade) (Figure 12c).

The overall increasing ice coverage in the Antarctic since November 1978 has been reported by Cavalieri and others (1997) and Watkins and Simmonds (2000) for November 1978 – December 1996, by Stammerjohn and Smith (1997) for 1979-1994, and by Zwally and others (2002) for November 1978 – December 1998. This increase was preceded by sharp declines in the Antarctic sea ice coverage in the 1970s (Kukla and Gavin, 1981), and the extension of the SMMR/SSMI data record back to 1973 by incorporation of ESMR and NIC data reveals that the decreases in the 1970s were large enough that the overall 1973-2002 trend in Antarctic sea ice is negative despite the increases since the late 1970s (Folland and others, 2001; Cavalieri and others, 2003).

## 5. Interannual Variability of Sea Ice

Despite the statistically significant overall trends in the sea ice covers (Section 4), considerable interannual variability exists in both hemispheres, and this is true for each month of the year. Here we illustrate the interannual variability with a complete set of early summer ice cover images in both hemispheres (July in the Northern Hemisphere, January in the Southern Hemisphere) over the full 25 years.

### *a. Arctic*

Figure 13 presents images of July sea ice concentrations in the Northern Hemisphere in each year 1979-2003. Examination of any region shows interannual variability and no steady direction of change (toward increasing or decreasing sea ice coverage) through the 25 years. In Hudson Bay, which typically has a nearly complete ice cover in winter (e.g., Figures 6 and 7), ice with concentrations of at least 44% continued to cover a sizeable portion of the bay in July 1992, much of the south coastal area in July 1982, 1985, 1986, 1994, 1995, and 2000, but almost none of the bay in July of most of the

other years, with some Julys (1998, 1999, and 2001) showing practically no ice of any concentration (Figure 13). The Kara Sea has a comparable variability, with, for instance, July 1995 having practically no ice and July 1987 and 1999 having ice of at least 44% concentration throughout the sea (Figure 13). Similar variability can be seen in the other marginal seas and bays as well.

Polynyas are apparent in each of the 25 images of Figure 13; and although almost all of them are coastal polynyas, the sizes and locations vary widely. All years except 2000 show a polynya just north of Canada centered in the longitude range 120-135°W (just east of Mackenzie Bay), but the size of this polynya varies from only a few pixels (approximately 25 km x 25 km each) in some years to a considerable area, covering 4° of latitude and over 20° of longitude, in 1998. Along the north coast of Asia, 1990 stands out as having the most sizeable July polynyas, and 1996 stands out as having the most compact ice. As for the most famous of Arctic polynyas, the North Water Polynya just west of Greenland at 75-79°N is visible as a polynya in July of several of the years (e.g., 1979, 1980, 1998) but has broken out to become part of the open water expanse extending to the Atlantic in others of the years (e.g., 1985, 2000, 2002, 2003) (Figure 13).

*b. Antarctic*

To illustrate interannual variability in the Antarctic ice, Figure 14 presents images of January ice concentrations for each of the 25 years 1979-2003. As in the Arctic, all regions show significant interannual variability. In the western Weddell Sea, some Januarys show a prominent northeastward extension of the ice indicative of the influence of the clockwise Weddell Gyre (1979, 1980, 1989, 1995, 1996, 2001, and 2003), but others show no suggestion of this influence (e.g., 2000, 2002). The years 1980 and 1998 stand out for the lack of January ice in the southernmost portion of the western Weddell Sea, despite considerable ice further north (Figure 14).

In the Bellingshausen/Amundsen Seas, the one region of the Antarctic most notably "bucking the trend" toward increased sea ice coverage (Jacobs and Comiso, 1997; Stammerjohn and Smith, 1997; Parkinson, 2002; Zwally and others, 2002), 1979, 1980, and 1987 show ice along almost the

entire length of the west coast of the Antarctic Peninsula, whereas this coast is largely free of ice in 1989-1991 and 1999. The Amundsen Sea has coastal polynyas of various sizes in most Januarys, but by January of 1992 and 2003, these polynyas had vanished, as the ice cover had retreated to the point where open water extended unhindered from the coast northward (Figure 14).

A larger polynya than the Amundsen Sea ones typically exists off the Ross Ice Shelf in December, having been formed in either November or December (Figures 9 and 10) by winds or ocean currents pushing the ice northward (e.g., Bromwich and Kurtz, 1984). By January this polynya has often broken out to the open water to the north. In the 1979-2003 period, several January averages show a continuing polynya (e.g., 1982, 1996, 1999), others show a small breaking out of the earlier polynya to the open ocean (e.g., 1988, 1993), and many show a complete break out to the open ocean (including 1979, 1980, 1986, 1987, 1990, 1997, 2002). The one year showing a substantial ice cover remaining adjacent to the ice shelf and only a relatively small polynya is the final year of the record, 2003 (Figure 14).

All of these interannual variabilities, in both hemispheres, are tied in one way or another to variabilities in the atmosphere and ocean. In the next section, we mention a sampling of the many studies that have attempted to explain some of the variability of the ice covers by connecting the ice to various oscillations and other factors in the rest of the climate system.

**6. Discussion: Sea ice in the context of the climate system**

The satellite record has revealed considerable information about the polar sea ice covers, including details about the seasonal cycle (Section 3), much greater interannual variability (Section 5) than previously recognized, and various long-term trends (Section 4). Because sea ice is an active component of the global climate system, influencing and being influenced by the oceans and atmosphere (e.g., Section 1), its variability (Section 5) and trends (Section 4) are both presumably closely tied to variability and trends in the rest of the system. Quantifying the connections, however, has proven challenging. In this concluding section, we cite a sampling of the many attempts.

*a. Arctic*

The decreases in the Arctic sea ice cover over the past several decades (e.g., Figure 11) have generated particular attention because of possible connections with global warming (e.g., Vinnikov and others, 1999), and more specifically Arctic temperature increases (e.g., Chapman and Walsh, 1993), and because of possible impacts on polar wildlife (e.g., Stirling and Derocher, 1993; Gradinger, 1995) and humans (e.g., Arctic Climate Impact Assessment, 2004). Vinnikov and others (1999) use a 5000-year run of the NOAA Geophysical Fluid Dynamics Laboratory (GFDL) global climate model (GCM) to calculate that, based on "natural variability" as simulated by the GFDL GCM, the probability of obtaining as strong a trend as the satellite-derived decrease in Arctic sea ice extents for the 1978-1998 period is under 2%, if only natural variability is operating. Chapman and Walsh (1993) find the observed sea ice variations and their spatial patterns to be compatible with the 1961-1990 record of temperature changes, which show warming over most of the Arctic but cooling in southern Greenland and its vicinity. The Arctic Climate Impact Assessment (2004) and others raise concerns regarding the continued viability of the Arctic polar bear and other wildlife populations should the current warming and decreasing ice coverage continue.

Despite the difficulties inherent because of the brevity of the satellite record and the incompleteness of the pre-satellite record, many studies have suggested possible long-term oscillatory behavior in the Arctic sea ice cover, tied to oscillatory behaviors in the atmosphere and ocean. In particular, connections have been made between the sea ice cover and the North Atlantic Oscillation (NAO) (e.g., Hurrell and van Loon, 1997; Johannessen and others, 1999; Kwok and Rothrock, 1999; Deser and others, 2000; Kwok, 2000; Parkinson, 2000; Vinje, 2001), the spatially broader Arctic Oscillation (e.g., Deser and others, 2000; Wang and Ikeda, 2000), the Arctic Ocean Oscillation (e.g., Polyakov and others, 1999; Proshutinsky and others, 1999), and an interdecadal Arctic climate cycle (Mysak and others, 1990; Mysak and Power, 1992).

Of the oscillations, the NAO has received the most attention. The NAO index is often calculated as the normalized atmospheric pressure at Lisbon, Portugal, minus the normalized atmospheric

pressure at Stykkisholmur, Iceland. This index was positive, with strong Azores High and Icelandic Low pressure systems, during the 1980s and early 1990s (Hurrell, 1995), resulting in strong southwesterly winds across the North Atlantic, bringing warm air to the Barents and Kara Seas and the central Arctic, and strong north winds over Baffin Bay and the Labrador Sea, bringing cold air to those regions, consistent with the pattern of temperature trends found by Chapman and Walsh (1993). Also consistent, as the NAO index increased during the 1980s, ice extents to the east and north of Greenland tended to decrease and ice extents to the west of Greenland, in Baffin Bay, the Labrador Sea, and Hudson Bay, tended to increase, whereas during the 1990s, as the NAO index decreased, ice extents to the east and north of Greenland tended to increase and those to the west of Greenland tended to decrease (Parkinson, 2000). Convincing as the overall summary is, however, the details of the ice changes, with their high interannual variability, and the brevity of the record make the results only suggestive of a sea ice/NAO connection, with further work needed before fully establishing and understanding the connection (Parkinson, 2000).

Most of the above studies are restricted to the past few decades. In analyzing the much longer 1901-1997 period, incorporating the limited pre-satellite data, Walsh and Chapman (2001) conclude that the Arctic sea ice extent has decreased substantially over this period as well as over the more recent period, with the stronger decreases over the long time span coming in the summer season. They further find the leading mode of wintertime variability to be dominated by a pattern consistent with forcing by the NAO (Walsh and Chapman, 2001).

*b. Antarctic*

The modes of atmospheric variability in the Southern Hemisphere include both symmetric and asymmetric patterns, and both have been examined for their impact on the sea ice cover. A large-scale, nearly zonally symmetric mode called the Southern Annular Mode (SAM), or the Antarctic Oscillation, is characterized by an alternation of atmospheric mass between middle and high southern latitudes (Rogers and van Loon, 1982). The SAM dominates the atmospheric circulation (Carleton,

2003) and influences the upper Southern Ocean circulation more than it does the Antarctic sea ice cover (Lefebvre and others, 2004), although there is evidence that extremes in the Antarctic sea ice cover impact atmospheric circulation in the summer, in particular such that the SAM tends toward positive polarity under minimum sea ice cover (Raphael, 2003). Model simulations suggest the SAM can generate sea ice variations on interannual to centennial time scales (Hall and Visbeck, 2002), although Lefebvre and others (2004) find no connection between the long-term trends in the Antarctic sea ice cover and the SAM index.

Asymmetric modes of atmospheric variability in the vicinity of Antarctica include a dominant wave 1 pattern observed in mean monthly surface air temperatures. The dominance of wave 1 in the temperature field results from the generally colder temperatures off the East Antarctic coast than those at comparable latitudes around the rest of Antarctica. This asymmetry results directly from the zonally asymmetric position of the Antarctic continent itself. Interestingly, higher wave numbers are more important in the sea level pressure field, where the first four wave numbers account for most of the variance (Cavalieri and Parkinson, 1981).

Many of the observed connections between atmospheric modes of variability and the Antarctic sea ice cover are regional in nature and are dominant in the Amundsen, Bellingshausen, and Weddell sea sectors (e.g., Yuan and Martinson, 2000; Stammerjohn and others, 2003). This results, at least in part, from the influence of the tropical El Niño/Southern Oscillation (ENSO). Sea ice-atmosphere linkages in the western Antarctic Peninsula region have been found to involve changes in the amplitude and phase of the semi-annual oscillation that also appear related to ENSO changes in the tropical Pacific (Stammerjohn and others, 2003). Significant retreats in the ice cover of the Amundsen and Bellingshausen seas were associated with four ENSO events over the 17 year period 1988-1994 (Kwok and Comiso, 2002). ENSO events typically occur every 2-7 years. In a study of coupled oscillations in Antarctic sea ice and the atmosphere over the South Pacific, Venegas and others (2001) found interannual oscillations with 3-6 year periods to have dominated wintertime sea ice and atmosphere variability in the Bellingshausen, Amundsen, and Ross Sea regions during the period

1979-1998. This result is consistent with the earlier work of Gloersen (1995) showing statistically significant periodicities in both the Antarctic sea ice cover and the ENSO index but considerable variability in the sea ice response for different regions. In particular, Gloersen (1995) found a dominant quasi-quadrennial period of about 4.2 years in the Weddell Sea sector, a strong biennial component in the Bellingshausen-Amundsen Sea sector, and a strong quasi-triennial component in the Ross Sea sector.

Rind and others (2001) simulate, in a theoretical modeling study, that El Niño events should produce lowered sea ice coverage in the Pacific portion of the Southern Ocean. Using data from approximately 18 years of observations, Yuan and Martinson (2000) find that up to 34% of the observed sea ice extent anomaly variance is linearly related to ENSO, but that even higher correlations exist between sea ice edge anomalies and tropical Pacific precipitation and sea surface temperature in the Indian Ocean. They further find that correlations between sea ice edge anomalies and global surface temperature produce four significant correlation patterns, with some extending into the tropics and the Northern Hemisphere.

The variations of the atmospheric long waves are an integral part of many hypothesized and observed ice/atmosphere connections. Among the identified patterns, there is a wave 1 mode represented by an oscillation in pressure between the Weddell and East Antarctic sectors; and there is a wave 2 mode that is strongest in the Pacific and southwest Atlantic sectors, perhaps influenced by the ENSO (Carleton, 2003), and that manifests itself as the Antarctic Circumpolar Wave observed in a range of variables in the ice-ocean-atmosphere system (White and Peterson, 1996). Also tied to the ENSO, a quasi-stationary wave in the southern high latitudes with centers in the Atlantic and Pacific has been identified and named the Antarctic Dipole by Yuan and Martinson (2000, 2001), who found that the Dipole exhibits high temperatures and low sea ice in the Pacific and low temperatures and high sea ice in the Atlantic during an El Niño and the opposite conditions during a la Niña (see also Yuan, 2004, for an overview of the connections among the Antarctic Dipole, ENSO, and Antarctic sea

ice). Other work suggests that a quasi-stationary atmospheric wave 3 pattern dominates the winter season and strongly impacts the wintertime sea ice distribution (Yuan and others, 1999).

A full understanding of the physical mechanisms explaining these various interconnections between the sea ice cover and the atmosphere and oceans does not yet exist. This is true for both the Arctic and the Antarctic and includes such fundamental issues as whether there should be a polar amplification of climate change (e.g., see Parkinson, 2004). Many studies have quantified connections for specific regions and time periods, but the picture remains far from unified and complete. Satellite monitoring of the ice cover has led to a greatly improved understanding of the seasonal cycle, trends, and interannual variability of the ice over the period of the satellite record (Sections 3-5), and continued satellite monitoring of the ice and other elements of the climate system should contribute eventually to improved understandings of the various interconnections and thereby to the possibility of improved predictions.

**Acknowledgments**

We thank Nick DiGirolamo and Al Ivanoff for their skill and patience in generating the figures through numerous iterations, the U.S. National Snow and Ice Data Center (NSIDC) for archiving and distributing the sea ice data sets, and the Cryospheric Sciences Program at NASA Headquarters for funding the work.

**References**

Ainley, D. G., C. T. Tynan, and I. Stirling, 2003, Sea ice: A critical habitat for polar marine mammals and birds, *in* Sea Ice: An Introduction to Its Physics, Chemistry, Biology and Geology (edited by D. N. Thomas and G. S. Dieckmann), Oxford, Blackwell Science, p. 240-266.

Arctic Climate Impact Assessment, 2004, *Impacts of a Warming Arctic: Arctic Climate Impact Assessment*, Cambridge, United Kingdom, Cambridge University Press, 140 p.

Arctic Climatology Project, 2000, Environmental Working Group Joint U.S.-Russian Sea Ice Atlas (edited by F. Tanis and V. Smolyanitsky), Boulder, Colorado, National Snow and Ice Data Center, CD-ROM.

Arrigo, K. R., G. L. Van Dijken, D. G. Ainley, M. A. Fahnestock, and T. Markus, 2002, Ecological impact of a large Antarctic iceberg, *Geophysical Research Letters*, v. 29, 10.1029/2001GL014160.

Bjørgo, E., O. M. Johannessen, and M. W. Miles, 1997; Analysis of merged SMMR-SSMI time series of Arctic and Antarctic sea ice parameters 1978-1995, *Geophysical Research Letters*, v. 24, no. 4, p. 413-416.

Bromwich, D. H., and D. D. Kurtz, 1984, Katabatic wind forcing of the Terra Nova Bay polynya, *Journal of Geophysical Research*, v. 89, no. C3, p. 3561-3572.

Carleton, A. M., 2003, Atmospheric teleconnections involving the Southern Ocean, *Journal of Geophysical Research*, v. 108, no. C4, 8080, doi:10.1029/2000JC000379.

Cavalieri, D. J., P. Gloersen, and W. J. Campbell, 1984, Determination of sea ice parameters with the Nimbus-7 SMMR, *Journal of Geophysical Research*, v. 89, p. 5355-5369.

Cavalieri, D. J., P. Gloersen, C. L. Parkinson, J. C. Comiso, and H. J. Zwally, 1997, Observed hemispheric asymmetry in global sea ice changes, *Science*, v. 272, p. 1104-1106.

Cavalieri, D. J., and C. L. Parkinson, 1981, Large-scale variations in observed Antarctic sea ice extent and associated atmospheric circulation, *Monthly Weather Review*, v. 109, p. 2323-2336.

Cavalieri, D. J., C. L. Parkinson, P. Gloersen, J. C. Comiso, and H. J. Zwally, 1999, Deriving long-term time series of sea ice cover from satellite passive-microwave multisensor data sets, *Journal of Geophysical Research*, v. 104, p. 15,803-15,814.

Cavalieri, D. J., C. L. Parkinson, and K. Y. Vinnikov, 2003, 30-Year satellite record reveals contrasting Arctic and Antarctic decadal sea ice variability, *Geophysical Research Letters*, v. 30, no. 18, 1970, doi:10.1029/2003GL018031.

Chapman, W. L., and J. E. Walsh, 1993, Recent variations of sea ice and air temperature in high latitudes, *Bulletin of the American Meteorological Society*, v. 74, no. 1, p. 33-47.

Colony, R., and A. S. Thorndike, 1984, *Arctic Ocean Drift Tracks from Ships, Buoys and Manned Research Stations, 1872-1973,* Boulder, Colorado, National Snow and Ice Data Center. Digital media.

Comiso, J. C., D. J. Cavalieri, and T. Markus, 2003, Sea ice concentration, ice temperature, and snow depth using AMSR-E data, *IEEE Transactions on Geoscience and Remote Sensing*, v. 41, p. 243-252.

Croxall, J. P., P. N. Trathan, and E. J. Murphy, 2002, Environmental change and Arctic seabird populations, *Science*, v. 297, p. 1510-1514.

Dehn, W., 2002, *Arctic Sea Ice Charts, 1953-1986: W. Dehn Collection*, Boulder, Colorado, National Snow and Ice Data Center. Digital media.

Derocher, A. N., N. J. Lunn, and I. Stirling, 2004, Polar bears in a warming climate, *Integrative and Comparative Biology*, v. 44, p. 163-176.

Deser, C., J. E. Walsh, and M. S. Timlin, 2000, Arctic sea ice variability in the context of recent atmospheric circulation trends, *Journal of Climate*, v. 13, p. 617-633.

Fetterer, F., and V. Troisi, 1997, *AARI 10-Day Arctic Ocean EASE-Grid Sea Ice Observations*, Boulder, Colorado, National Snow and Ice Data Center. Digital media.

Folland, C. K., T. R. Karl, J. R. Christy, R. A. Clarke, G. V. Gruza, J. Jouzel, M. E. Mann, J. Oerlemans, M. J. Salinger, and S.-W. Wang, 2001, Observed climate variability and change, in

*Climate Change 2001: The Scientific Basis. Contribution of Working Group I to the Third Assessment Report of the Intergovernmental Panel on Climate Change* (edited by J. T. Houghton, Y. Ding, D. J. Griggs, M. Noguer, P. J. van der Linden, X. Dai, K. Maskell, and C. A. Johnson), Cambridge, United Kingdom, Cambridge University Press, p. 99-181.

Fowler, C., 2003, *Polar Pathfinder Daily 25 km EASE-Grid Sea Ice Motion Vectors*, Boulder, Colorado, National Snow and Ice Data Center. Digital media.

Gloersen, P., 1995, Modulations of hemispheric sea-ice cover by ENSO events, *Nature*, v. 373, p. 503-506.

Gloersen, P., and F. T. Barath, 1977, A scanning multichannel microwave radiometer for Nimbus-G and SeaSat-A, *IEEE Journal of Oceanic Engineering*, v. OE-2, no. 2, p. 172-178.

Gloersen, P., W. J. Campbell, D. J. Cavalieri, J. C. Comiso, C. L. Parkinson, and H. J. Zwally, 1992, *Arctic and Antarctic Sea Ice, 1978-1987: Satellite Passive-Microwave Observations and Analysis*, NASA SP-511, Washington, D. C., National Aeronautics and Space Administration, 290 p.

Gloersen, P., C. L. Parkinson, D. J. Cavalieri, J. C. Comiso, and H. J. Zwally, 1999, Spatial distribution of trends and seasonality in the hemispheric sea ice covers: 1978-1996, *Journal of Geophysical Research*, v. 104, p. 20,827-20,836.

Gradinger, R., 1995, Climate change and biological oceanography of the Arctic Ocean, *Philosophical Transactions of the Royal Society of London*, Series A, v. 352, p.277-286.

Grumet, N.S., C. P. Wake, P. A. Mayewski, G. A. Zielinski, S. I. Whitlow, R. M. Koerner, D. A. Fisher, and J. M. Woollett, 2001, Variability of sea-ice extent in Baffin Bay over the last millennium, *Climate Change*, v. 49, no. 1-2, p. 129-145.

Hall, A., and M. Visbeck, 2002, Synchronous variability in the Southern Hemisphere atmosphere, sea ice, and ocean resulting from the annular mode, *Journal of Climate*, v. 15, p. 3043-3057.

Hall, D. K., J. R. Key, K. A. Casey, G. A. Riggs, and D. J. Cavalieri, 2004, Sea ice surface temperature product from the Moderate Resolution Imaging Spectroradiometer (MODIS), *IEEE Transactions on Geoscience and Remote Sensing*, v. 42, p. 1076-1087.

Hill, B. T., A. Ruffman, and K. Drinkwater, 2002, Historical record of the incidence of sea ice on the Scotian Shelf and the Gulf of St. Lawrence, in *Ice in the Environment: Proceedings of the 16th IAHR International Symposium on Ice*, Dunedin, New Zealand, 2nd–6th December 2002, International Association of Hydraulic Engineering and Research, p. 16-24.

Hurrell, J. W., 1995, Decadal trends in the North Atlantic Oscillation: Regional temperatures and precipitation, *Science*, v. 269, p. 676-679.

Hurrell, J. W., and H. van Loon, 1997, Decadal variations in climate associated with the North Atlantic Oscillation, *Climatic Change*, v. 36, no. 3, p. 301-326.

Ito, H., 1982, *Sea Ice Atlas of Northern Baffin Bay*, Zurich, Switzerland, Department of Geography, Swiss Federal Institute of Technology Zurich, 142 p.

Jacobs, S. S., and J. C. Comiso, 1997, Climate variability in the Amundsen and Bellingshausen Seas, *Journal of Climate*, v. 10, no. 4, p. 697-709.

Jeffries, M. O., S. Li, R. A. Jaña, H. R. Krouse, and B. Hurst-Cushing, 1998, Late winter first-year ice floe thickness variability, seawater flooding and snow ice formation in the Amundsen and Ross seas, in *Antarctic Sea Ice: Physical Processes, Interactions and Variability* (edited by M. O. Jeffries), Washington, D. C., American Geophysical Union, Antarctic Research Series, v. 74, p. 69-87.

Jevrejeva, S., 2001, Severity of winter seasons in the northern Baltic Sea between 1529 and 1990: Reconstruction and analysis, *Climate Research,* v. 17, p. 55-62.

Johannessen, O. M., M. Miles, and E. Bjørgo, 1995, The Arctic's shrinking sea ice, *Nature*, v. 376, no. 6536, p. 126-127.

Johannessen, O. M., E. V. Shalina, and M. W. Miles, 1999, Satellite evidence for an Arctic sea ice cover in transformation, *Science*, v. 286, p. 1937-1939.

Kawanishi, T., T. Sezai, Y. Ito, K. Imaoka, T. Takeshima, Y. Ishido, A. Shibata, M. Miura, H. Inahata, and R. W. Spencer, 2003, The Advanced Microwave Scanning Radiometer for the Earth Observing System (AMSR-E), NASDA's contribution to the EOS for global energy and water cycle studies, *IEEE Transactions on Geoscience and Remote Sensing*, v. 41, no. 2, p. 184-194.

Key, J., and M. Haefliger, 1992, Arctic ice surface temperature retrieval from AVHRR thermal channels, *Journal of Geophysical Research*, v. 97, no. D5, p. 5885-5893.

Koch, L., 1945, The East Greenland ice, *Medd Groenl*, v. 130, no. 3, p. 1-374.

Kukla, G., and J. Gavin, 1981, Summer ice and carbon dioxide, *Science*, v. 214, no. 4520, p. 497-503.

Kwok, R., 2000, Recent changes in Arctic Ocean sea ice motion associated with the North Atlantic Oscillation, *Geophysical Research Letters*, v. 27. no. 6, p. 775-778.

Kwok, R., and J. C. Comiso, 2002, Spatial patterns of variability in Antarctic surface temperature: Connections to the Southern Hemisphere Annular Mode and the Southern Oscillation, *Geophysical Research Letters*, v. 29, no. 14, 10.1029/2002GL015415.

Kwok, R., and D. A. Rothrock, 1999, Variability of Fram Strait ice flux and North Atlantic Oscillation, *Journal of Geophysical Research*, v. 104, no. C3, p. 5177-5189.

LeDrew, E., D. Barber, T. Agnew, and D. Dunlap, 1992, *Canadian Sea Ice Atlas From Microwave Remotely Sensed Imagery: July 1987 to June 1990*, Ottawa, Canada, Canada Communication Group – Publishing, 80 p.

Lefebvre, W., H. Goosse, R. Timmermann, and T. Fichefet, 2004, Influence of the Southern Annular Mode on the sea ice-ocean system, *Journal of Geophysical Research,* v. 109, no. C9, C09005, doi:10.1029/2004JC002403.

Liu, A. K., Y. Zhao, and S. Y. Wu, 1999, Arctic sea ice drift from wavelet analysis of NSCAT and special sensor microwave imager data, *Journal of Geophysical Research*, v. 104, p. 11,529-11,538.

Long, D.G., P. Hardin, and P. Whiting, 1993, Resolution enhancement of spaceborne scatterometer data, *IEEE Transactions on Geoscience and Remote Sensing*, v. 31, p. 700-715.

Massom, R. A., 1991, *Satellite Remote Sensing of Polar Regions*, London, Belhaven Press, 307 p.

Maykut, Gary A., 1978, Energy exchange over young sea ice in the central Arctic, *Journal of Geophysical Research*, v. 83, no. C7, p. 3646-3658.

McLaren, A. S., J. E. Walsh, R. H. Bourke, R. L. Weaver, and W. Wittmann, 1992, Variability in sea-ice thickness over the North Pole from 1977 to 1990, *Nature*, v. 358, p. 224-226.

Melnikov, I. A., 1997, *The Arctic Sea Ice Ecosystem*: Amsterdam, Gordon and Breach Science Publishers, 204 p.

Mysak, L. A., and S. B. Power, 1992, Sea-ice anomalies in the western Arctic and Greenland-Iceland Sea and their relation to an interdecadal climate cycle, *Climatological Bulletin/Bulletin Climatologique*, v. 26, no. 3, p. 147-176.

Mysak, L. A., D. K. Manak, and R. F. Marsden, 1990, Sea-ice anomalies observed in the Greenland and Labrador Seas during 1901-1984 and their relation to an interdecadal Arctic climate cycle, *Climate Dynamics*, v. 5, p. 111-133.

NSIDC, compiler, 1999, *Polar Pathfinder sampler: AVHRR, SMMR-SSM/I, and TOVS samples and combined time series*: Boulder, Colorado, National Snow and Ice Data Center. CD-ROM.

NSIDC, 2004, *Morphometric Characteristics of Ice and Snow in the Arctic Basin: Aircraft Landing Observations from the Former Soviet Union, 1928-1989* (I. P. Romanov, compiler): Boulder, Colorado, National Snow and Ice Data Center. Digital media.

Parkinson, C. L., 2000, Recent trend reversals in Arctic sea ice extents: Possible connections to the North Atlantic Oscillation, *Polar Geography*, v. 24, no. 1, p. 1-12.

Parkinson, C. L., 2002, Trends in the length of the Southern Ocean sea-ice season, 1979-99, *Annals of Glaciology*, v. 34, p. 435-440.

Parkinson, C. L., 2004, Southern Ocean sea ice and its wider linkages: Insights revealed from models and observations, *Antarctic Science*, vol. 16, no. 4, p. 387-400, doi:10.1017/S0954102004002214.

Parkinson, C. L., D. J. Cavalieri, P. Gloersen, H. J. Zwally, and J. C. Comiso, 1999, Variability of the Arctic sea ice cover 1978-1996, *Journal of Geophysical Research*, v. 104, p. 20,837-20,856.

Parkinson, C. L., J. C. Comiso, H. J. Zwally, D. J. Cavalieri, P. Gloersen, and W. J. Campbell, 1987, *Arctic Sea Ice, 1973-1976: Satellite Passive-Microwave Observations*: NASA SP-489, Washington, D. C., National Aeronautics and Space Administration, 296 p.

Poe, G., K. St. Germain, J. Bobak, S. Swadley, J. Wessel, B. Thomas, J. Wang, and B. Burns, 2001, *DMSP Calibration/Validation Plan for the Special Sensor Microwave Imager Sounder (SSMIS)*, unpublished report, 28 November 2001, Washington, D. C., Naval Research Laboratory, 190 p.

Polyakov, I. V., G. V. Alekseev, R. V. Bekryaev, U. S. Bhatt, R. Colony, M. A. Johnson, V. P. Karklin, D. Walsh, and A. V. Yulin, 2003, Long-term ice variability in Arctic marginal seas, *Journal of Climate*, v. 16, no. 12, p. 2078-2085.

Polyakov, I. V., A. Y. Proshutinsky, and M. A. Johnson, 1999, Seasonal cycles in two regimes of Arctic climate, *Journal of Geophysical Research*, v. 104, no. C11, p. 25,761-25,788.

Proshutinsky, A. Y., I. V. Polyakov, and M. A. Johnson, 1999, Climate states and variability of Arctic ice and water dynamics during 1946-1997, *Polar Research*, v. 18, no. 2, p. 135-142.

Raphael, M. N., 2003, Impact of observed sea-ice concentration on the Southern Hemisphere extratropical atmospheric circulation in summer, *Journal of Geophysical Research,* v. 108, no. D22, 4687, doi:10.1029/2002JD003308.

Riggs, G. A., D. K. Hall, and V. V. Salomonson, 2003, *MODIS Sea Ice User's Guide*, http://modis-snow-ice.gsfc.nasa.gov/siugkc.html.

Rind, D., M. Chandler, J. Lerner, D. G. Martinson, and X. Yuan, 2001, Climate response to basin-specific changes in latitudinal temperature gradients and implications for sea ice variability, *Journal of Geophysical Research*, v. 106, p. 20,161-20,173.

Rogers, J. C., and H. van Loon, 1982, Spatial variability of sea level pressure and 500 mb height anomalies over the Southern Hemisphere, *Monthly Weather Review*, v. 110, p. 1375-1392.

Rothrock, D. A., Y. Yu, and G. A. Maykut, 1999, Thinning of the Arctic sea-ice cover, *Geophysical Research Letters*, v. 26, no. 23, p. 3469-3472.

Schnack-Schiel, S. B., 2003, The macrobiology of sea ice, in *Sea Ice: An Introduction to Its Physics, Chemistry, Biology and Geology* (edited by D. N. Thomas and G. S. Dieckmann), Oxford, Blackwell Science, p. 211-239.

Stammerjohn, S. E., M. R. Drinkwater, R. C. Smith, and X. Liu, 2003, Ice-atmosphere interactions during sea-ice advance and retreat in the western Antarctic Peninsula region, *Journal of Geophysical Research,* v. 108, no. C10, 3329, doi:10.1029/2002JC001543.

Stammerjohn, S. E., and R. C. Smith, 1997, Opposing Southern Ocean climate patterns as revealed by trends in regional sea ice coverage, *Climatic Change*, v. 37, no. 4, p. 617-639.

Stirling, I., and A. E. Derocher, 1993, Possible impacts of climate warming on polar bears, *Arctic*, v. 46, no. 3, p. 240-245.

Venegas, S. A., M. R. Drinkwater, and G. Shaffer, 2001, Coupled oscillations in Antarctic sea ice and atmosphere in the South Pacific sector, *Geophysical Research Letters*, v. 28, p. 3301-3304.

Vinje, T., 2001, Anomalies and trends of sea-ice extent and atmospheric circulation in the Nordic Seas during the period 1864-1998, *Journal of Climate*, v. 14, p. 255-267.

Vinnikov, K. Y., A. Robock, R. J. Stouffer, J. E. Walsh, C. L. Parkinson, D. J. Cavalieri, J. F. B. Mitchell, D. Garrett, and V. F. Zakharov, 1999, Global warming and Northern Hemisphere sea ice extent, *Science*, v. 286, p. 1934-1937.

Vyas, N. K., S. M. Bhandari, M. K. Dash, P. C. Pandey, N. Khare, A. Khanolkar, and N. Sharma, 2004, *An Atlas of Antarctic Sea Ice from Oceansat-1 MSMR (June 1999 – September 2001)*, Gao, India, National Centre for Antarctic and Ocean Research, 64 p.

Wadhams, P., and N. R. Davis, 2000, Further evidence of ice thinning in the Arctic Ocean, *Geophysical Research Letters*, v. 27, no. 24, p. 3973-3975.

Walsh, J. E., and W. L. Chapman, 2001, 20th-century sea-ice variations from observational data, *Annals of Glaciology*, v. 33, p. 444-448.

Walsh, J. E., and C. M. Johnson, 1979, An analysis of Arctic sea ice fluctuations, 1953-77, *Journal of Physical Oceanography*, v. 9, no. 3, 580-591.

Wang, J. and M. Ikeda, 2000, Arctic Oscillation and Arctic Sea-Ice Oscillation, *Geophysical Research Letters*, v. 27, no. 9, p. 1287-1290.

Watkins, A. B., and I. Simmonds, 2000, Current trends in Antarctic sea ice: The 1990s impact on a short climatology, *Journal of Climate*, v. 13, no. 24, p. 4441-4451.

White, W. B., and R. G. Peterson, 1996, An Antarctic circumpolar wave in surface pressure, wind, temperature and sea ice extent, *Nature*, v. 380, p. 699-702.

Wingham, D.J., C.R. Francis, S. Baker, C. Bouzinac, R. Cullen, P. de Chateau-Thierry, S.W. Laxon, U. Mallow, C. Mavrocordatos, L. Phalippou, G. Ratier, L. Rey, F. Rostan, P. Viau, and D. Wallis, 2004, CryoSat: A mission to determine the fluctuations in Earth's land and marine ice fields, *Advances in Space Research*, submitted.

Winsor, P., 2001, Arctic sea ice thickness remained constant during the 1990s, *Geophysical Research Letters*, v. 28, no. 6, p. 1039-1041.

Worby, A. P., M. O. Jeffries, W. F. Weeks, K. Morris, and R. Jaña, 1996, The thickness distribution of sea ice and snow cover during late winter in the Bellingshausen and Amundsen Seas, Antarctica, *Journal of Geophysical Research*, v. 101, no. C12, p. 28,411-28,455.

Worby, A. P., R. A. Massom, I. Allison, V. I. Lytle, and P. Heil, 1998, East Antarctic sea ice: A review of its structure, properties and drift, in *Antarctic Sea Ice: Physical Processes, Interactions and Variability* (edited by M. O. Jeffries), Washington, D. C., American Geophysical Union, Antarctic Research Series, v. 74, p. 41-67.

Yuan, X., 2004, ENSO-related impacts on Antarctic sea ice: A synthesis of phenomenon and mechanisms, *Antarctic Science*, v. 16, no. 4, p. 415-425.

Yuan, X. and D. G. Martinson, 2000, Antarctic sea ice extent variability and its global connectivity, *Journal of Climate*, v. 3, p. 1697-1717.

Yuan, X., and D. G. Martinson, 2001, The Antarctic Dipole and its predictability, *Geophysical Research Letters*, v. 28, p. 3609-3612.

Yuan, X., D. G. Martinson, and W. T. Liu, 1999, Effect of air-sea-ice interaction on winter 1996 Southern Ocean subpolar storm distribution, *Journal of Geophysical Research,* v. 104, p. 1991-2007.

Zwally, H. J., J. C. Comiso, C. L. Parkinson, W. J. Campbell, F. D. Carsey and P. Gloersen, 1983, *Antarctic Sea Ice, 1973-1976: Satellite Passive-Microwave Observations*, NASA SP-459, Washington, D.C., National Aeronautics and Space Administration, 206 p.

Zwally, H. J., J. C. Comiso, C. L. Parkinson, D. J. Cavalieri, and P. Gloersen, 2002, Variability of Antarctic sea ice 1979-1998, *Journal of Geophysical Research*, v. 107, no. C5, 10.1029/2000JC000733.

Zwally, H. J., R. Schutz, C. Bentley, J. Bufton, T. Herring, J. Minster, J. Spinhirne, and R. Thomas, 2003, updated current year. *GLAS/ICESat L2 Sea Ice Altimetry Data V018*, 15 October to 18 November 2003, Boulder, Colorado, National Snow and Ice Data Center. Digital media.

**Figure Captions**

Figure 1. North polar location map and monthly sea ice distributions in March (white and light blue) and September (white), averaged over the 25 years 1979-2003. The sea ice distributions are derived from satellite data discussed in Section 3.

Figure 2. South polar location map and monthly sea ice distributions in February (white) and September (white and light blue), averaged over the 25 years 1979-2003. The sea ice distributions are derived from satellite data discussed in Section 3.

Figure 3. (a) NOAA 17 AVHRR image of the Bering Sea for March 13, 2003. (b) NIC sea ice analysis chart for the week of March 14, 2003.

Figure 4. Landsat 7 ETM+ image of St. Matthew Island in the Bering Sea on March 13, 2003. The image shows the detailed structure of the sea ice edge in the vicinity of the island.

Figure 5. Left: The Arctic region on March 12, 2003, as imaged from the 89 GHz vertically polarized channel of the EOS Aqua AMSR-E, at a spatial resolution of 5 km. Right: Ice surface temperature in Fram Strait on March 12, 2003, as determined from data of the EOS Terra MODIS. (Images from Hall and others, 2004.)

Figure 6. Monthly average sea ice concentrations in the Northern Hemisphere for January – December 2001, as derived from data of the DMSP SSMI.

Figure 7. Monthly average sea ice concentrations in the Northern Hemisphere for January – December, averaged over the 25-year period 1979-2003, as derived from data of the Nimbus 7 SMMR and the DMSP SSMI.

Figure 8. The 2001 (dashed lines) and 1979-2003 25-year average (solid lines) annual cycles of sea ice extents for the Northern Hemisphere (NH), the Southern Hemisphere (SH), and the total (Global).

Figure 9. Monthly average sea ice concentrations in the Southern Hemisphere for January – December 2001, as derived from data of the DMSP SSMI.

Figure 10. Monthly average sea ice concentrations in the Southern Hemisphere for January – December, averaged over the 25-year period 1979-2003, as derived from data of the Nimbus 7 SMMR and the DMSP SSMI.

Figure 11. (a) Monthly average ice extents in the Northern Hemisphere, November 1978 – December 2003. (b) Monthly ice-extent deviations in the Northern Hemisphere, November 1978 – December 2003. (c) Yearly and seasonal average ice extents in the Northern Hemisphere, 1979-2003. Winter (W) is averaged over January-March; spring (Sp) is averaged over April-June; summer (Su) is averaged over July-September; and autumn (A) is averaged over October-December. All values are derived from data of the Nimbus 7 SMMR and the DMSP SSMI. (Updated from Parkinson and others, 1999.)

Figure 12. (a) Monthly average ice extents in the Southern Hemisphere, November 1978 – December 2003. (b) Monthly ice-extent deviations in the Southern Hemisphere, November 1978 – December 2003. (c) Yearly and seasonal average ice extents in the Southern Hemisphere, 1979-2003. Summer (Su) is averaged over January-March; autumn (A) is averaged over April-June; winter (W) is averaged over July-September; and spring (Sp) is averaged over October-December. All values are derived from data of the Nimbus 7 SMMR and the DMSP SSMI. (Updated from Zwally and others, 2002.)

Figure 13. Monthly average July sea ice concentrations in the Northern Hemisphere for each year 1979-2003, as derived from data of the Nimbus 7 SMMR and the DMSP SSMI.

Figure 14. Monthly average January sea ice concentrations in the Southern Hemisphere for each year 1979-2003, as derived from data of the Nimbus 7 SMMR and the DMSP SSMI.

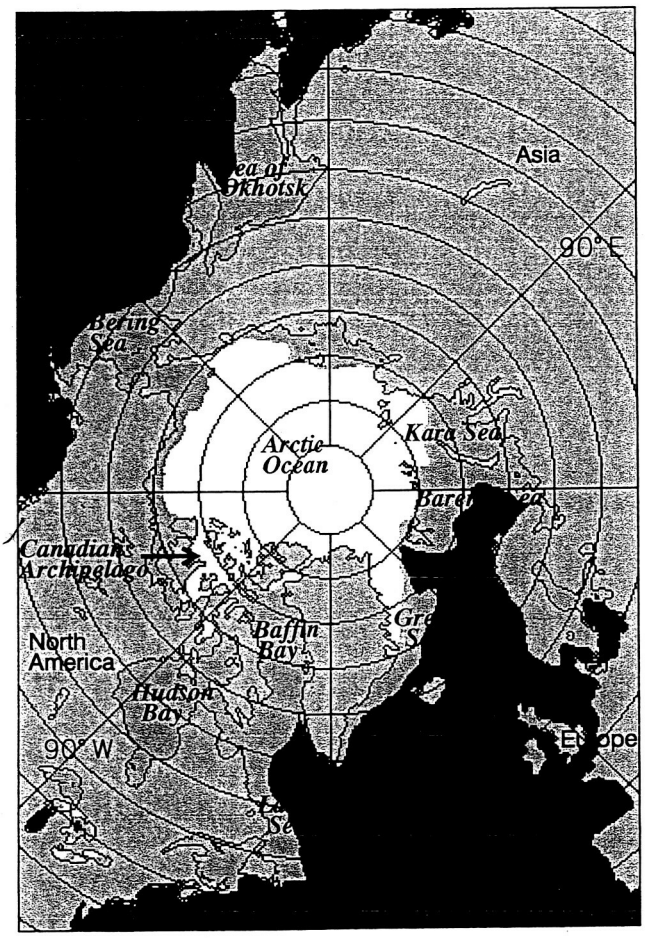
Asia
90° E
Arctic
Ocean
Kara Sea
Canadian
Archipelago
North
America
Baffin
Bay
Hudson
Bay
90° W

Figure 1

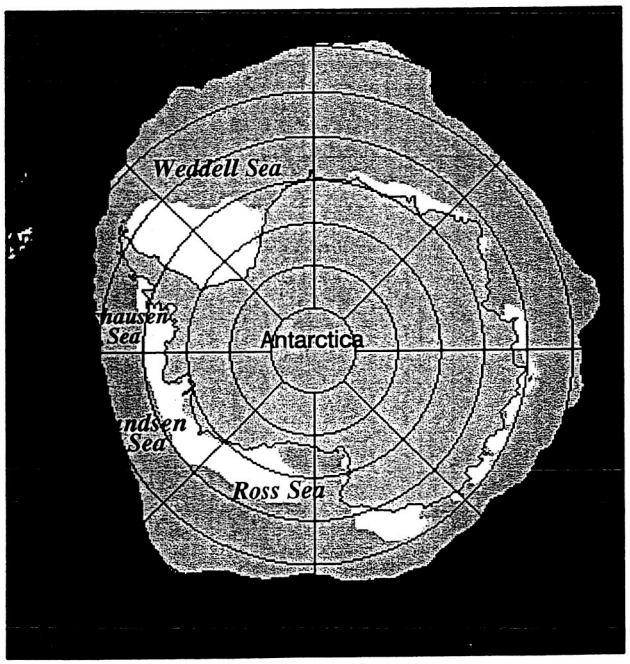


Figure 2

(a)

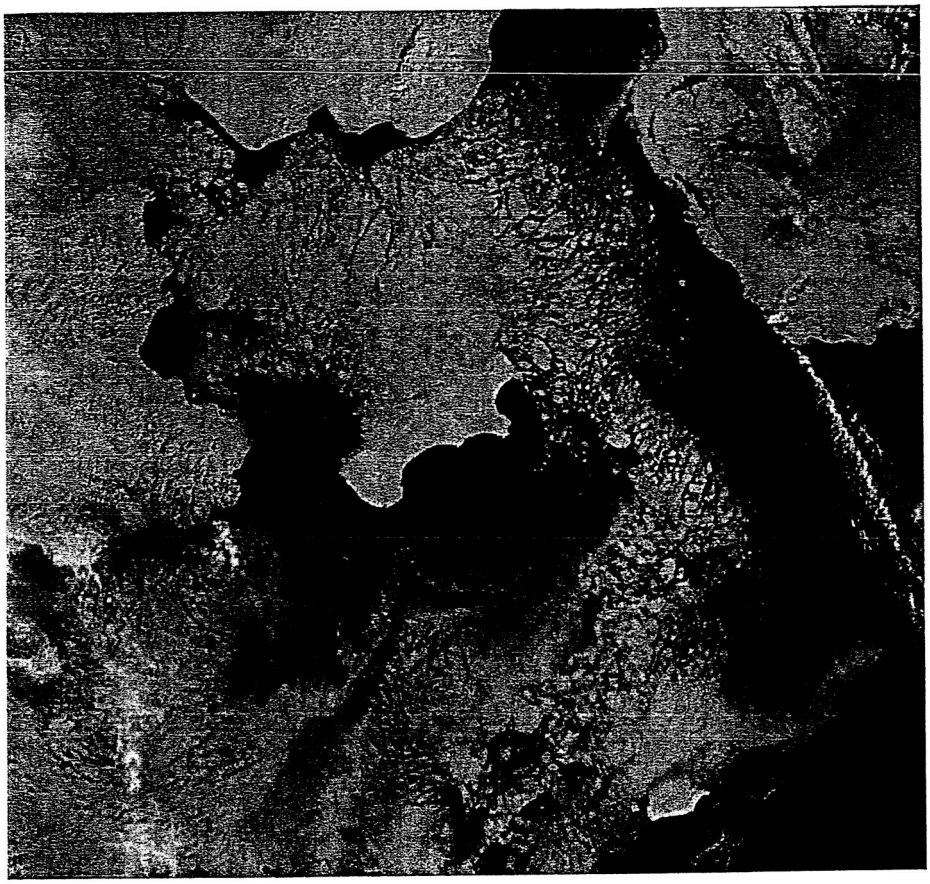

(b)

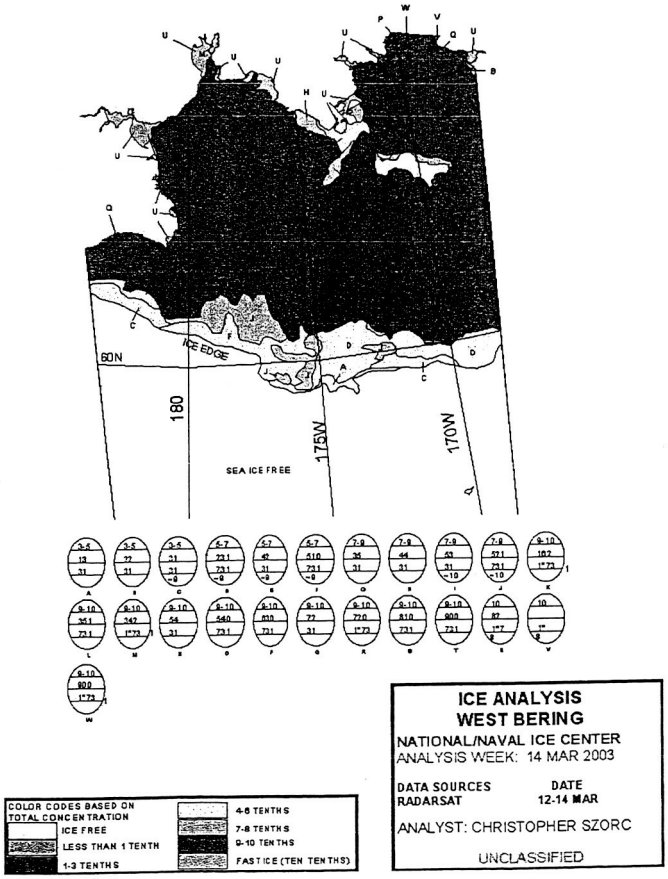
60N
ICE EDGE
180
175W
170W
SEA ICE FREE
COLOR CODES BASED ON TOTAL CONCENTRATION
ICE FREE
LESS THAN 1 TENTH
1-3 TENTHS
4-6 TENTHS
7-8 TENTHS
9-10 TENTHS
FAST ICE (TEN TENTHS)
ICE ANALYSIS
WEST BERING
NATIONAL/NAVAL ICE CENTER
ANALYSIS WEEK: 14 MAR 2003
DATA SOURCES
RADARSAT
DATE
12-14 MAR
ANALYST: CHRISTOPHER SZORC
UNCLASSIFIED

Figure 3

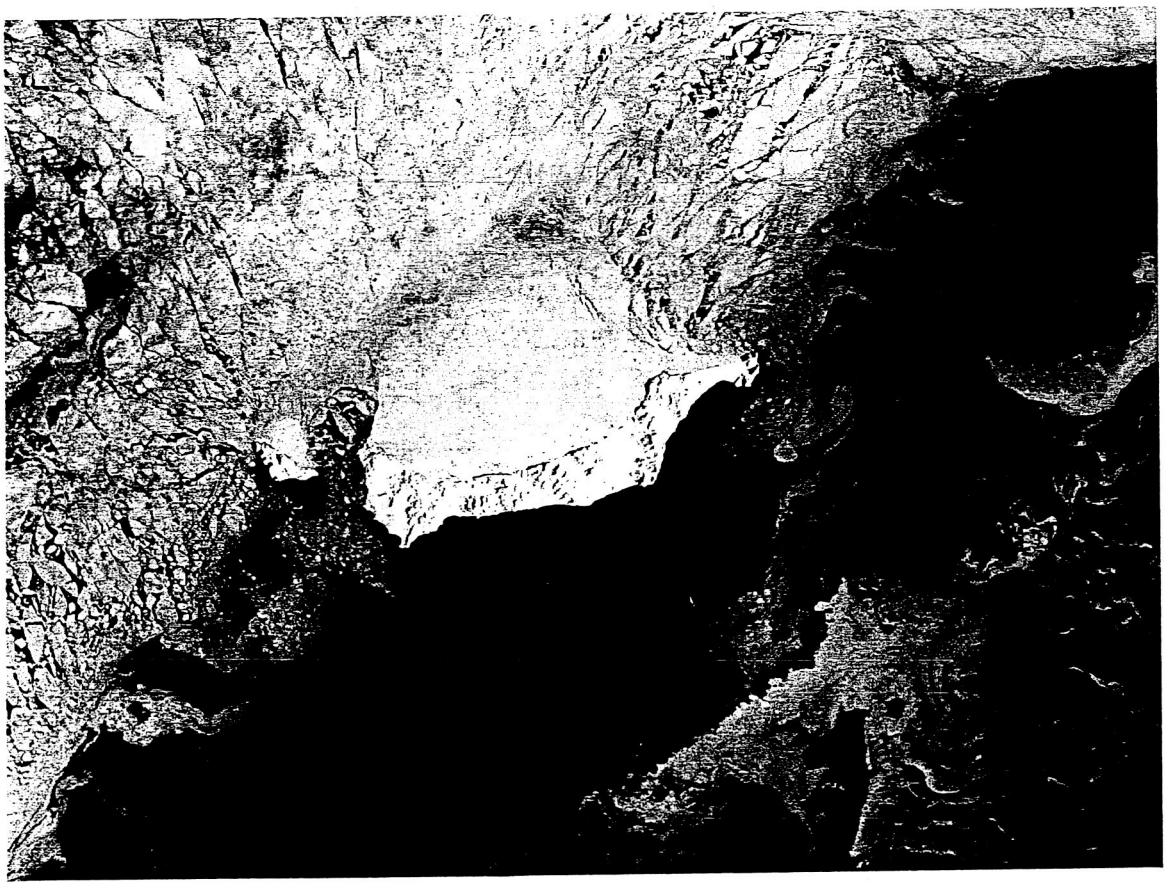

Figure 4

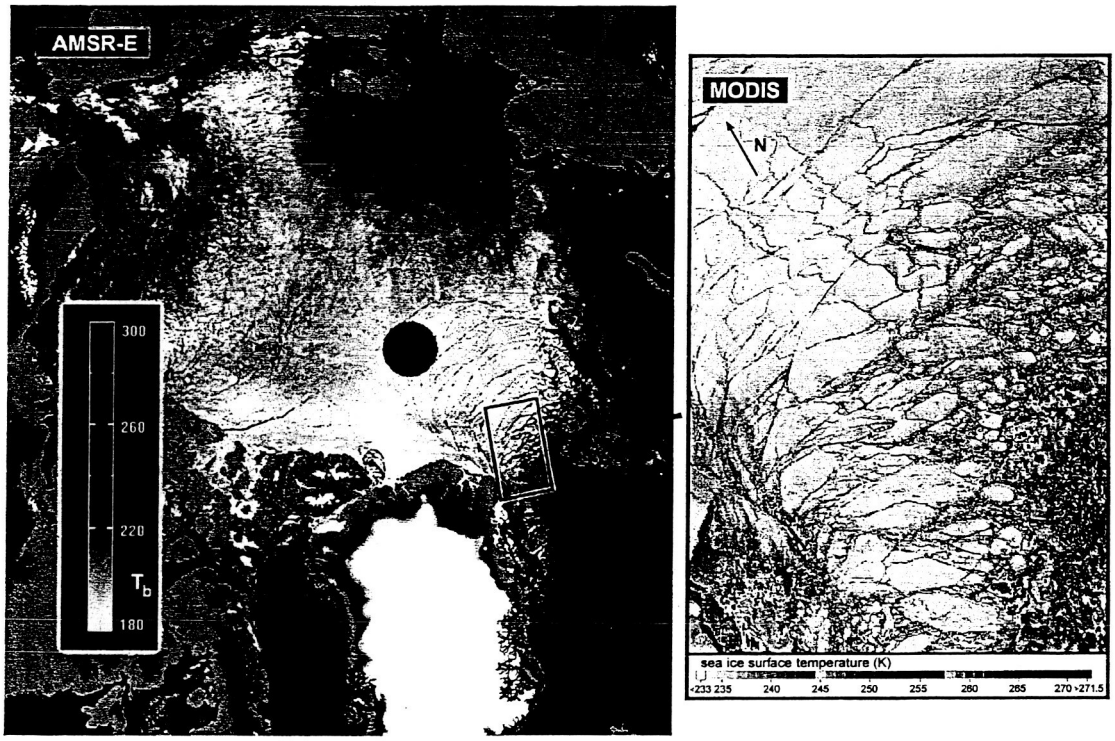
AMSR-E
300
260
220
$T_b$
180
MODIS
N
sea ice surface temperature (K)
233 235 240 245 250 255 260 265 270 271.5

Figure 5

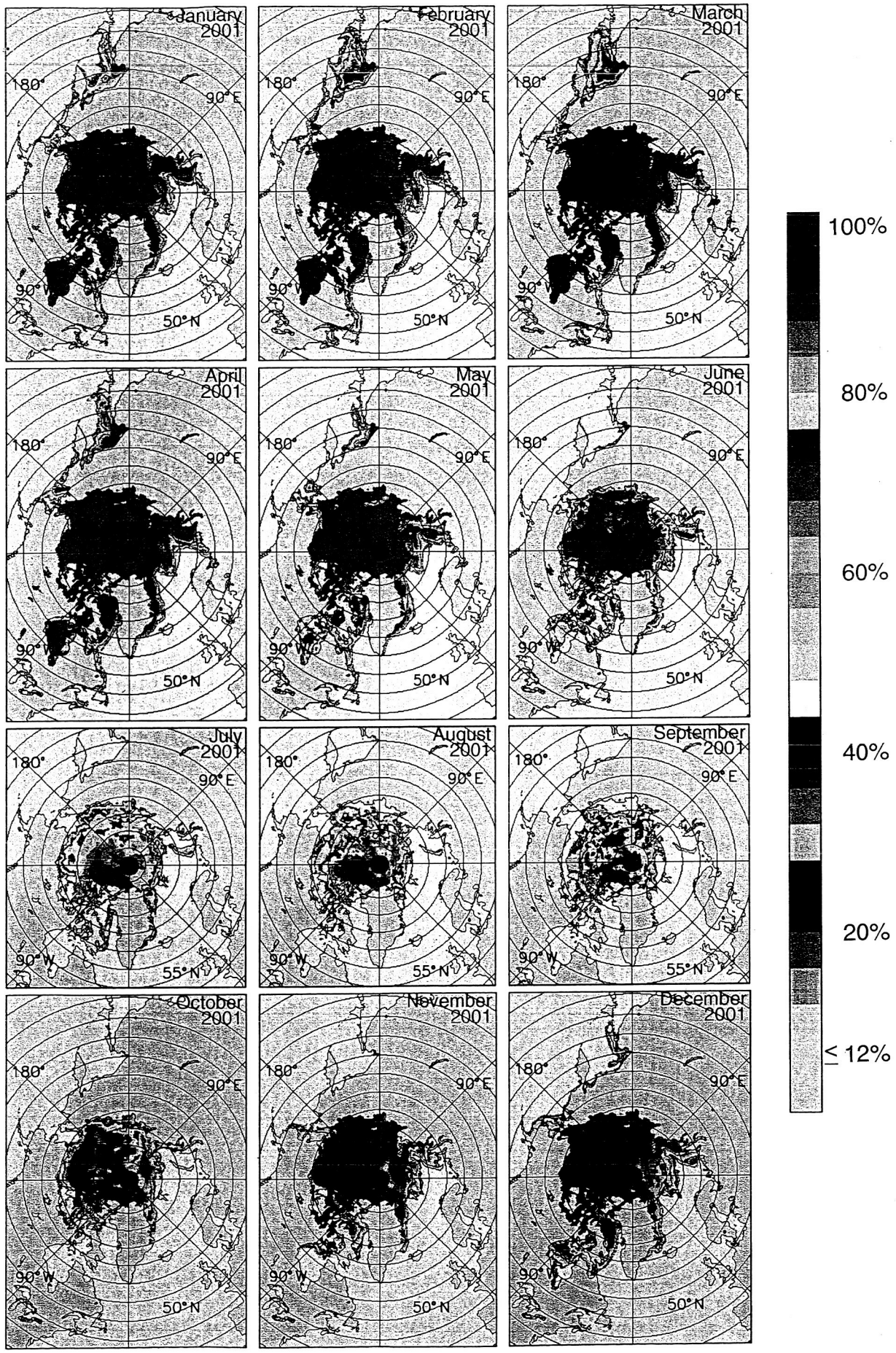
January 2001
February 2001
March 2001
April 2001
May 2001
June 2001
July 2001
August 2001
September 2001
October 2001
November 2001
December 2001
180°
90° E
90° W
50° N
55° N
100%
80%
60%
40%
20%
≤ 12%

Figure 6

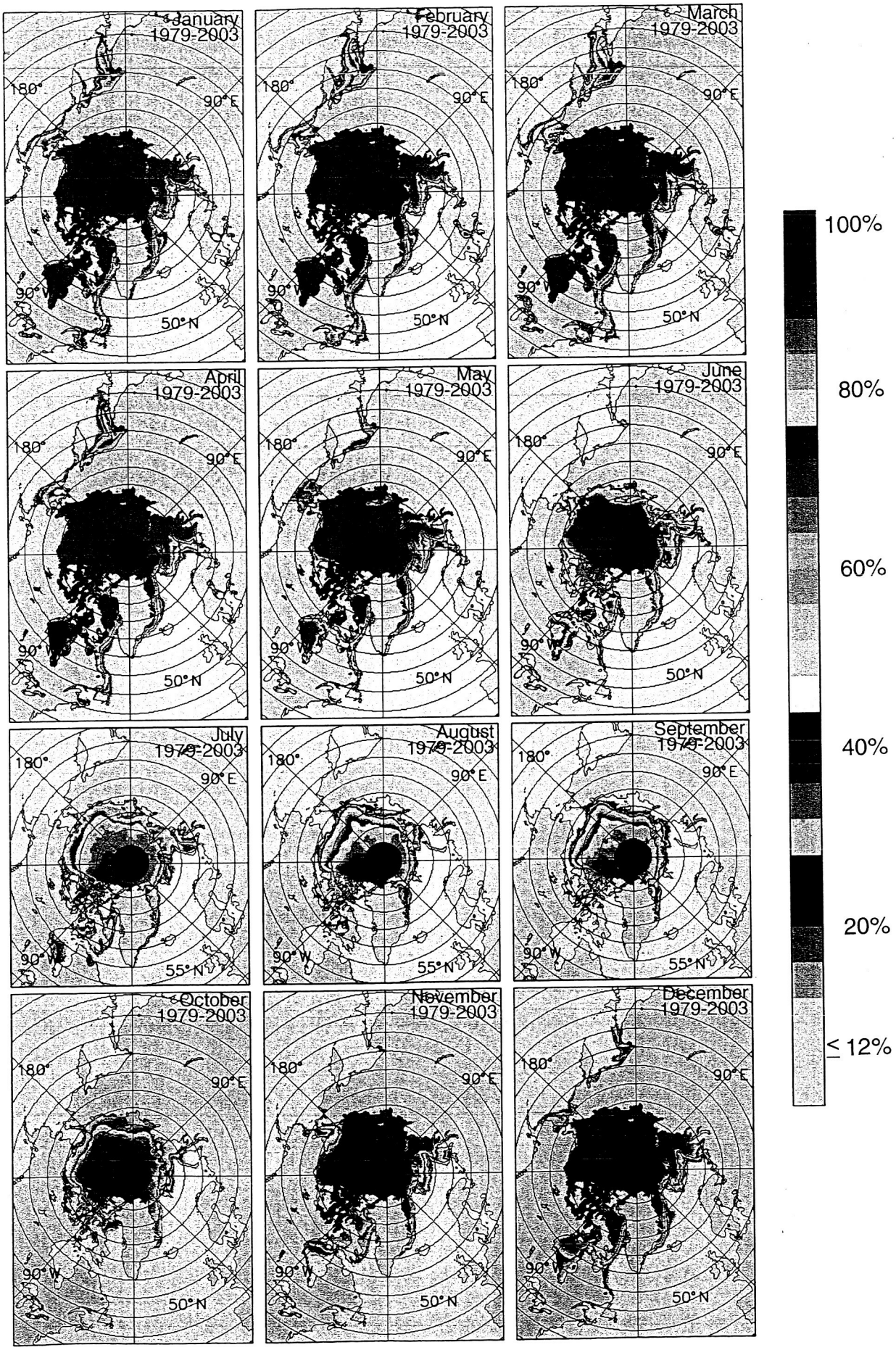
January
1979-2003
February
1979-2003
March
1979-2003
April
1979-2003
May
1979-2003
June
1979-2003
July
1979-2003
August
1979-2003
September
1979-2003
October
1979-2003
November
1979-2003
December
1979-2003
180°
90°E
90°W
50°N
55°N
100%
80%
60%
40%
20%
≤ 12%

Figure 7

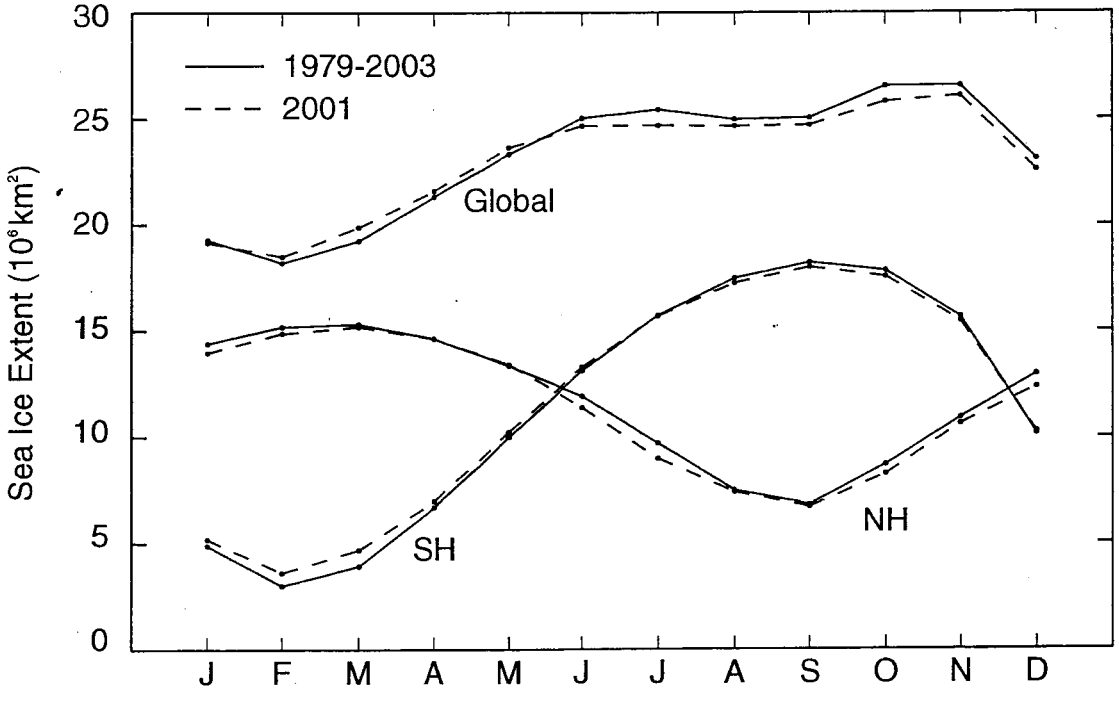
30
25
20
15
10
5
0
Sea Ice Extent ($10^6$ km$^2$)
1979-2003
2001
Global
NH
SH
J
F
M
A
M
J
J
A
S
O
N
D

Figure 8

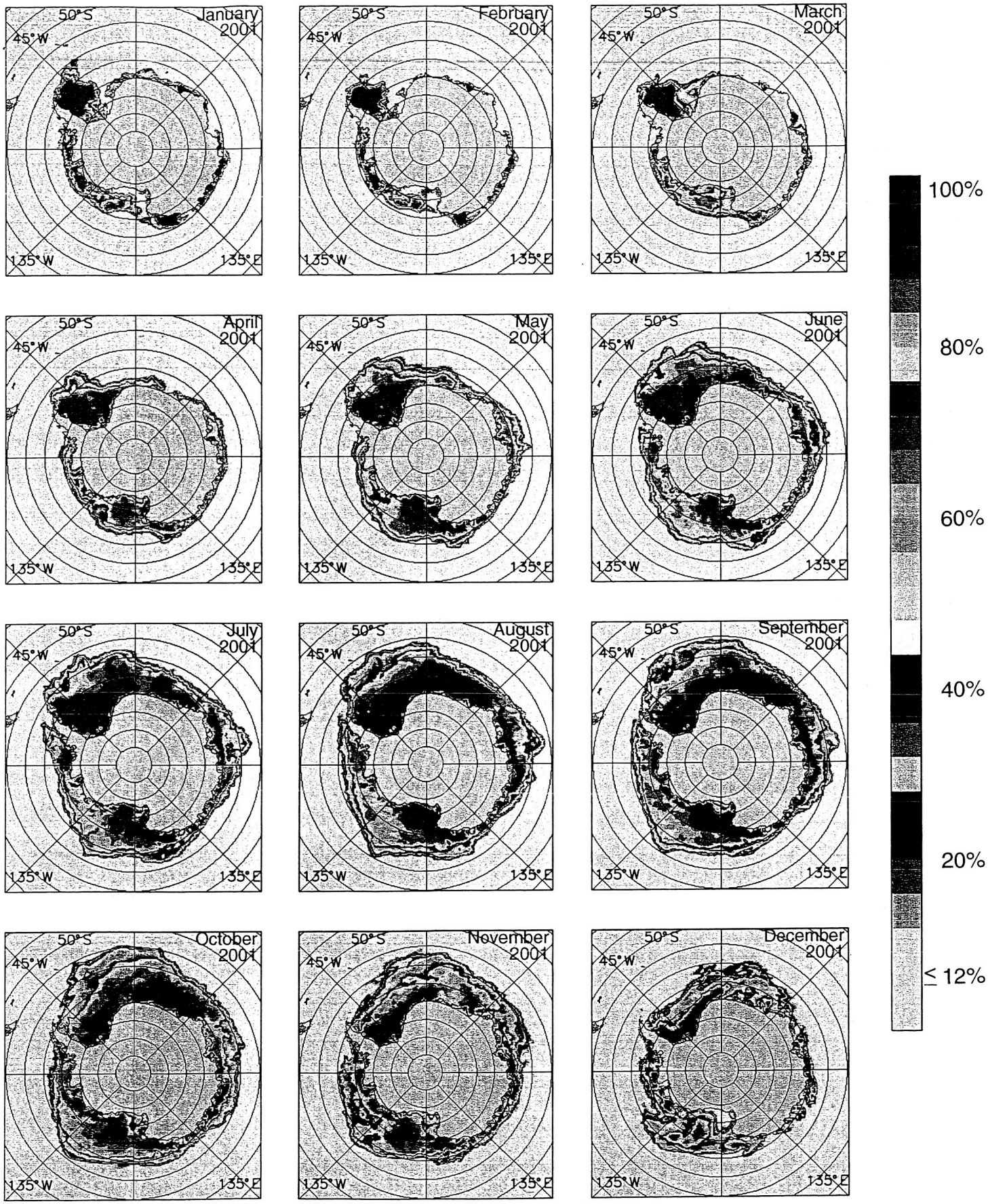
50°S
45°W
135°W
135°E
January 2001
February 2001
March 2001
April 2001
May 2001
June 2001
July 2001
August 2001
September 2001
October 2001
November 2001
December 2001
100%
80%
60%
40%
20%
≤ 12%

Figure 9

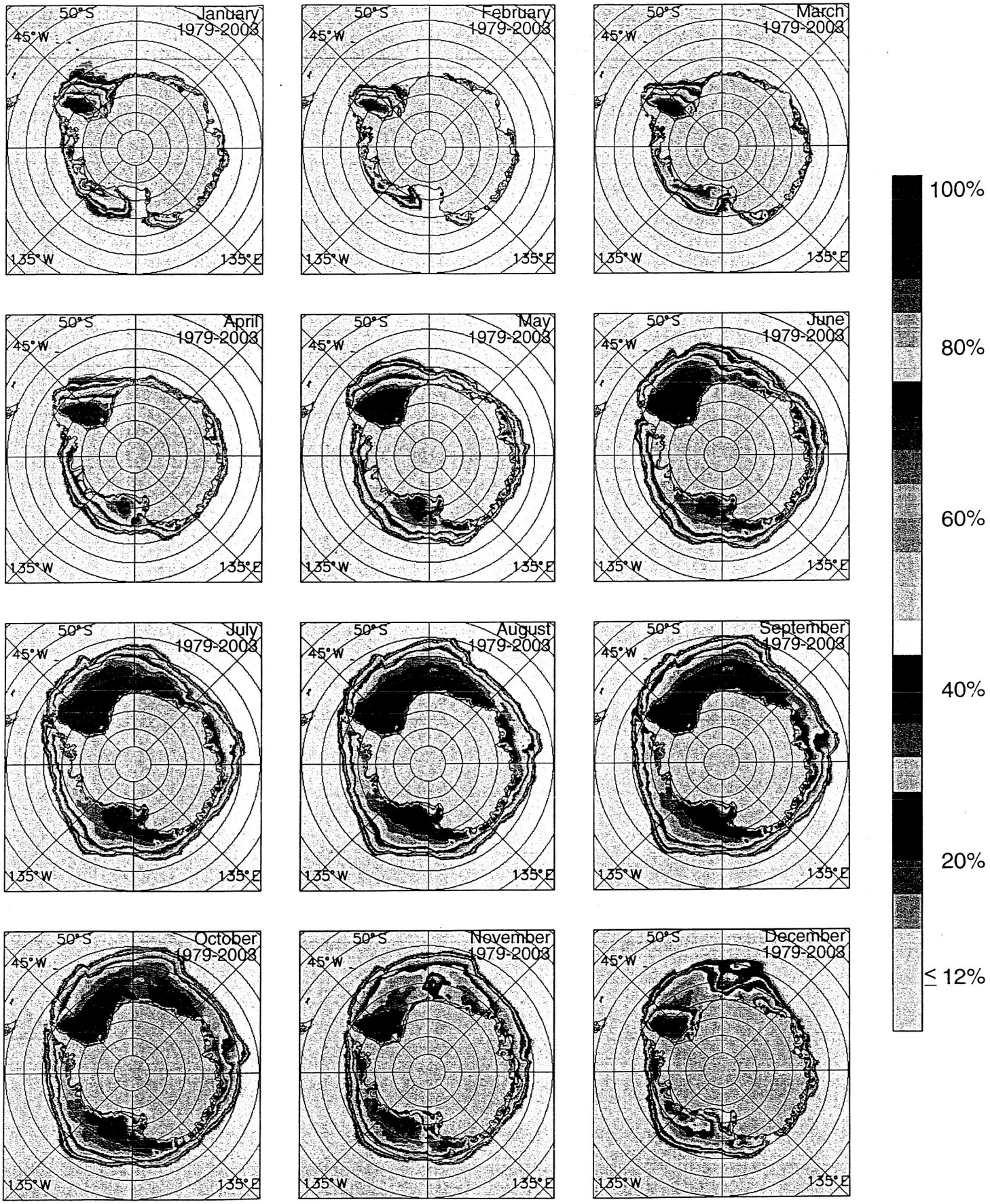
50°S
45°W
January
1979-2003
135°W
135°E
February
March
April
May
June
July
August
September
October
November
December
100%
80%
60%
40%
20%
≤ 12%

Figure 10

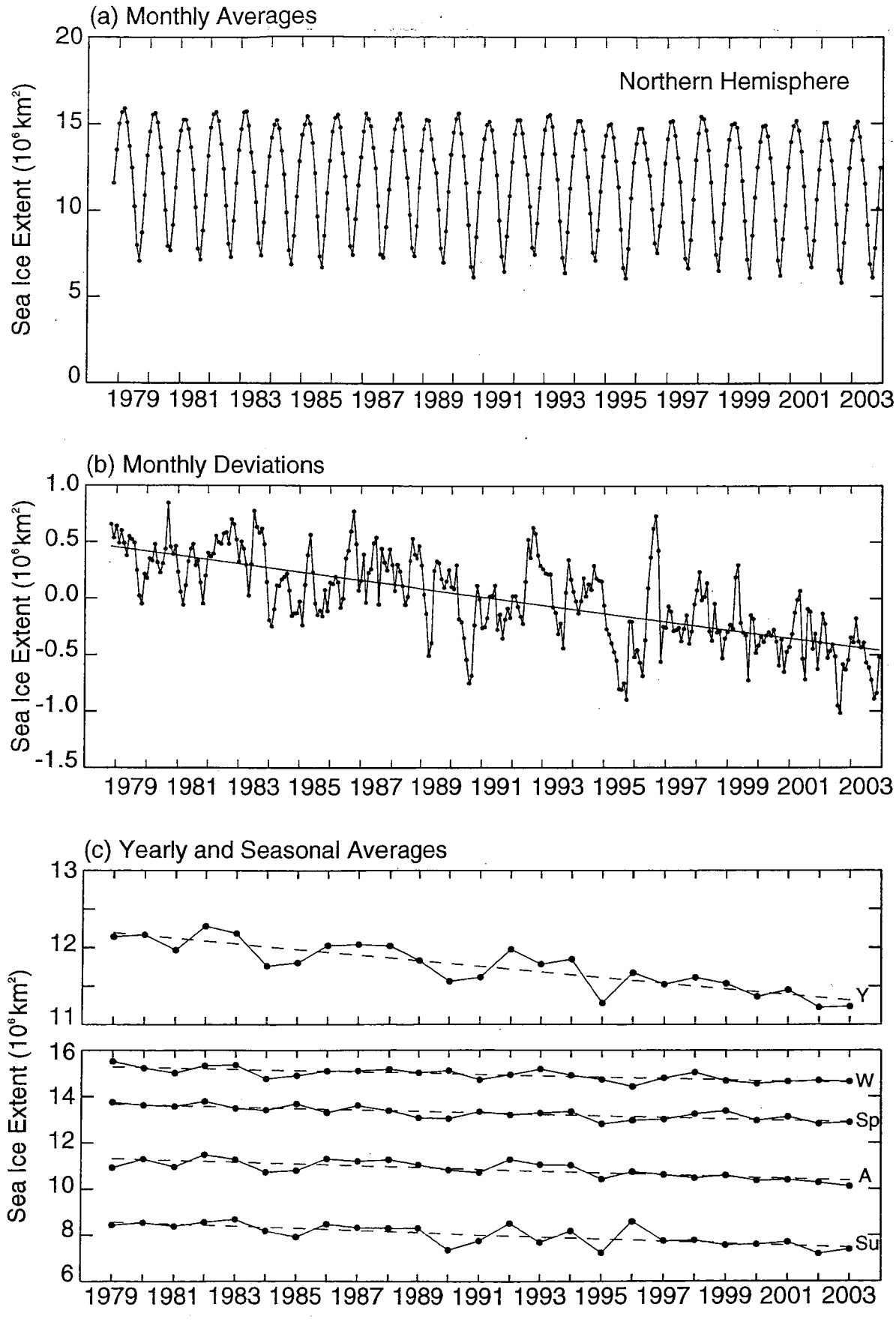
(a) Monthly Averages
Northern Hemisphere
Sea Ice Extent ($10^6$ km$^2$)
20
15
10
5
0
1979 1981 1983 1985 1987 1989 1991 1993 1995 1997 1999 2001 2003
(b) Monthly Deviations
Sea Ice Extent ($10^6$ km$^2$)
1.0
0.5
0.0
-0.5
-1.0
-1.5
1979 1981 1983 1985 1987 1989 1991 1993 1995 1997 1999 2001 2003
(c) Yearly and Seasonal Averages
Sea Ice Extent ($10^6$ km$^2$)
13
12
11
Y
16
14
12
10
8
6
W
Sp
A
Su
1979 1981 1983 1985 1987 1989 1991 1993 1995 1997 1999 2001 2003

Figure 11

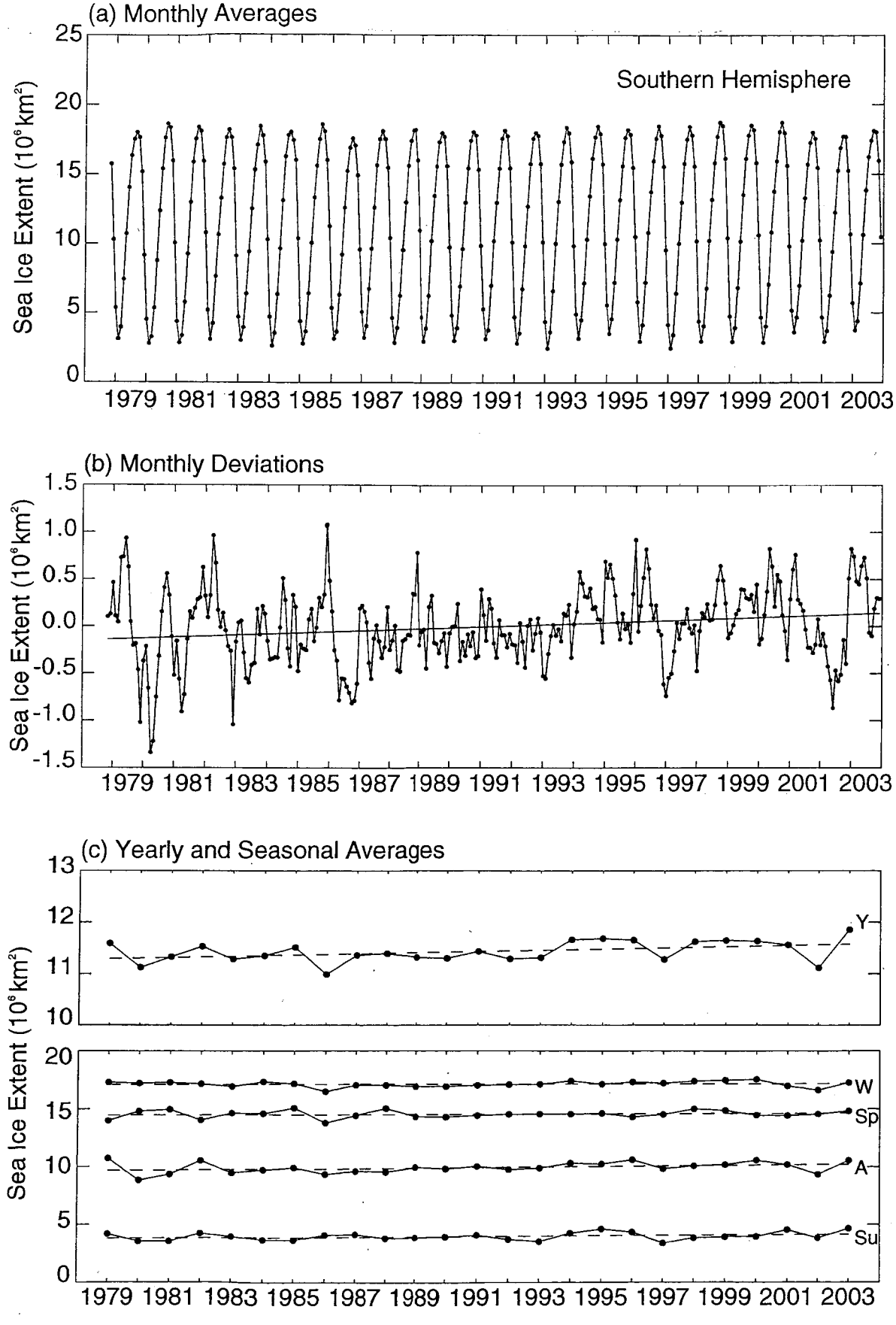
(a) Monthly Averages
Southern Hemisphere
Sea Ice Extent ($10^6$ km$^2$)
25
20
15
10
5
0
1979 1981 1983 1985 1987 1989 1991 1993 1995 1997 1999 2001 2003
(b) Monthly Deviations
Sea Ice Extent ($10^6$ km$^2$)
1.5
1.0
0.5
0.0
-0.5
-1.0
-1.5
1979 1981 1983 1985 1987 1989 1991 1993 1995 1997 1999 2001 2003
(c) Yearly and Seasonal Averages
Sea Ice Extent ($10^6$ km$^2$)
13
12
11
10
Y
20
15
10
5
0
W
Sp
A
Su
1979 1981 1983 1985 1987 1989 1991 1993 1995 1997 1999 2001 2003

Figure 12

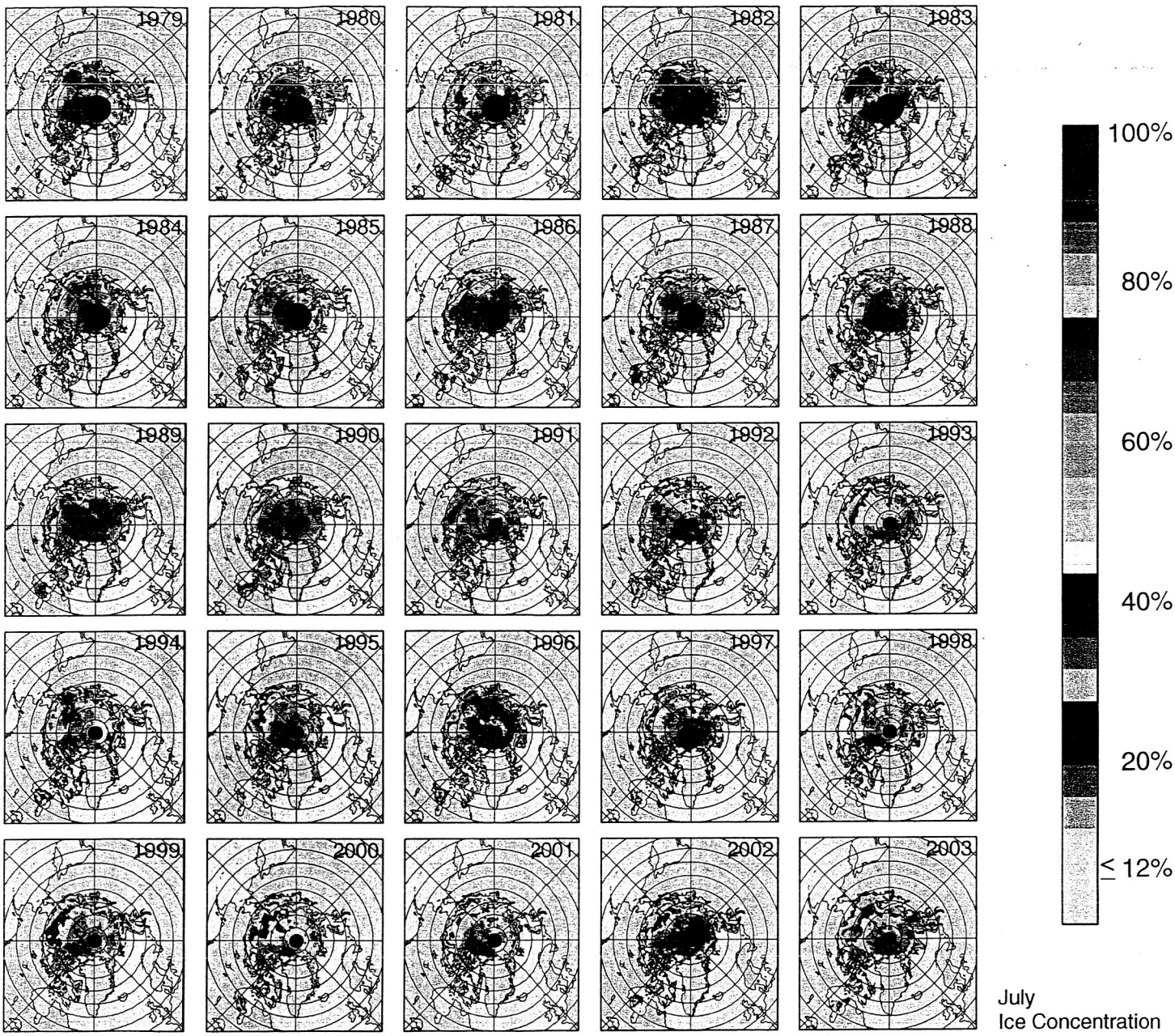
1979
1980
1981
1982
1983
1984
1985
1986
1987
1988
1989
1990
1991
1992
1993
1994
1995
1996
1997
1998
1999
2000
2001
2002
2003
100%
80%
60%
40%
20%
≤ 12%
July
Ice Concentration

Figure 13

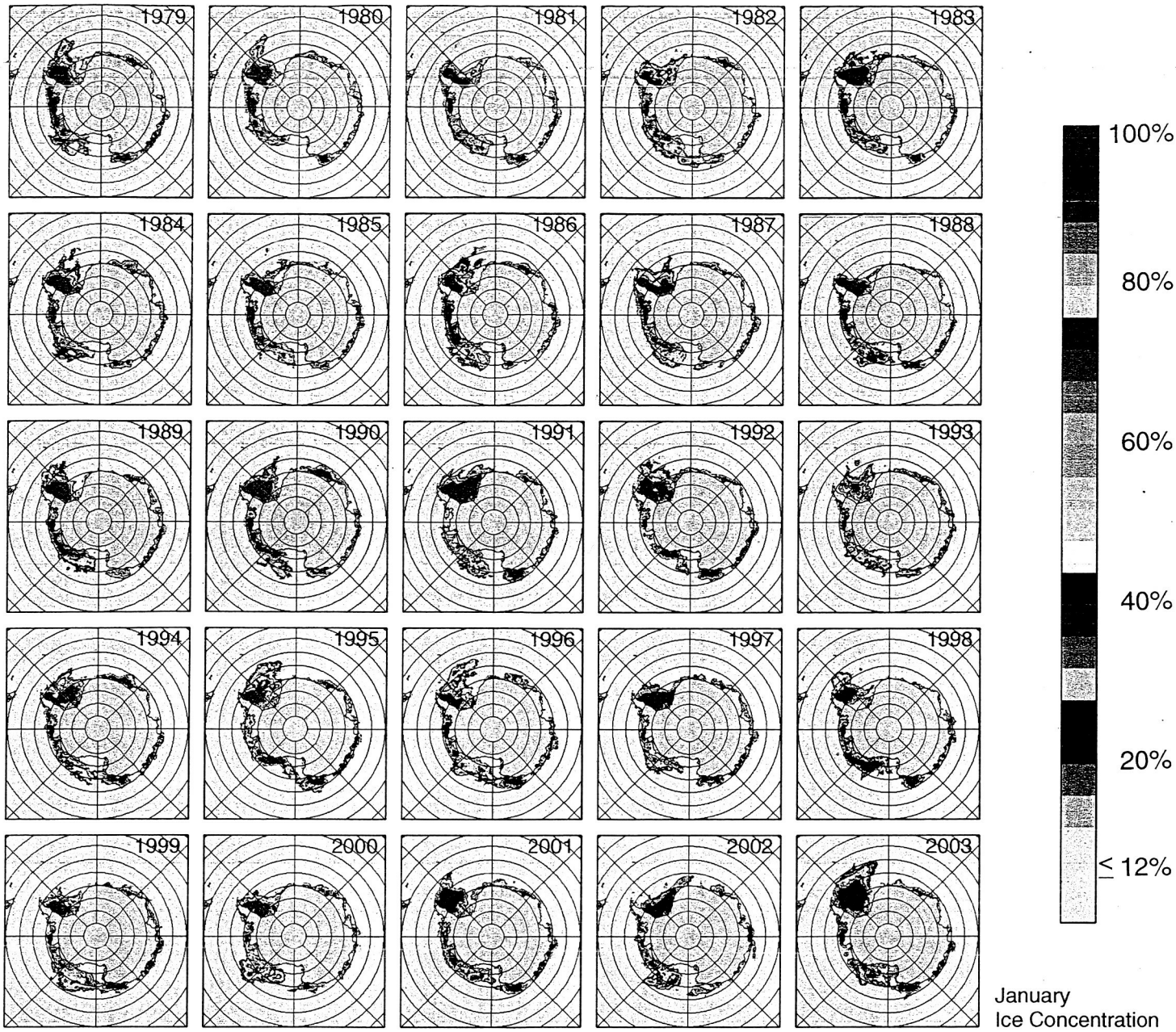
1979
1980
1981
1982
1983
1984
1985
1986
1987
1988
1989
1990
1991
1992
1993
1994
1995
1996
1997
1998
1999
2000
2001
2002
2003
100%
80%
60%
40%
20%
≤ 12%
January
Ice Concentration

Figure 14

*Satellite Image Atlas of Glaciers of the World*

*State of the Earth's Cryosphere at the Beginning of the 21st Century*

Sea Ice

*By* Claire L. Parkinson and Donald J. Cavalieri

Cryospheric Sciences Branch, NASA Goddard Space Flight Center

**Popular Summary**

Sea ice covers vast areas of the polar oceans, and in doing so, it restricts heat exchanges between the oceans and the atmosphere, reflects solar radiation back to space, and has multiple other impacts on the atmosphere, oceans, and ecosystems of the polar regions. In the first year of the twenty-first century, the areal extent of sea ice in the Northern Hemisphere ranged from a late summer value of $6.7 \times 10^6$ km$^2$ to a late winter value of $15.2 \times 10^6$ km$^2$ (more than one and a half times the area of the United States) and the areal extent of sea ice in the Southern Hemisphere ranged from a summer value of $3.6 \times 10^6$ km$^2$ to a winter value of $18.0 \times 10^6$ km$^2$. Satellite data for the period since late 1978 show that, overall, the sea ice coverage of the Northern Hemisphere has decreased, while the sea ice coverage of the Southern Hemisphere has shown lesser but still noticeable increases. The data reveal considerable variability from year to year and some intriguing possible connections with broader scale phenomena in the climate system, such as global warming, Arctic warming, El Niño, and various atmospheric-based oscillations termed the Arctic Oscillation, the North Atlantic Oscillation, and the Antarctic Oscillation. If the Arctic ice cover continues to decline, this could further speed the warming in the Arctic region and could harm the lifestyles of polar bears and other Arctic life forms.

*Satellite Image Atlas of Glaciers of the World*

*State of the Earth's Cryosphere at the Beginning of the 21st Century*

Sea Ice

*By* Claire L. Parkinson and Donald J. Cavalieri

Cryospheric Sciences Branch, NASA Goddard Space Flight Center

**Significant Findings**

This article is the sea ice chapter for a book on the *State of the Earth's Cryosphere at the Beginning of the 21st Century*. It therefore highlights the first year of the twenty-first century, providing detailed sea ice concentration maps for each month of 2001 for both the Northern and Southern Hemispheres. These maps, derived from satellite passive-microwave data, show the full annual cycles of the ice covers, including regional details of the ice concentrations and the locations and sizes of coastal and non-coastal polynyas. Integrating spatially, monthly ice extents in 2001 ranged in the Northern Hemisphere from $6.7 \times 10^6$ km$^2$ in September to $15.2 \times 10^6$ km$^2$ in March and in the Southern Hemisphere from $3.6 \times 10^6$ km$^2$ in February to $18.0 \times 10^6$ km$^2$ in September. The article also places the ice cover of 2001 in the context of the longer satellite passive-microwave record and provides updates, through the end of 2003, on the trends in hemispheric sea ice extents. Specifically, Northern Hemisphere ice extent trends are $-36{,}700 \pm 2{,}200$ km$^2$/yr for monthly deviations over the period November 1979 - December 2003 and $-36{,}600 \pm 4{,}400$ km$^2$/yr ($-3.0 \pm 0.4$ %/decade) for yearly averages over the period 1979-2003. The corresponding trends for the Southern Hemisphere are $11{,}200 \pm 3{,}100$ km$^2$/yr for monthly deviations and $11{,}700 \pm 5{,}400$ km$^2$/yr ($1.0 \pm 0.5$ %/decade) for yearly averages. I.e., the record reveals statistically significant ice extent decreases in the Northern Hemisphere and statistically significant ice extent increases in the Southern Hemisphere, but the Northern Hemisphere decreases are more than three times the magnitude of the Southern Hemisphere increases.